Available online at www.sciencedirect.com
ScienceDirect
Deep-Sea Research II 55 (2008) 820–840
DEEP-SEA RESEARCH PART II
www.elsevier.com/locate/dsr2

Insights into nutrient assimilation and export in naturally iron-fertilized waters of the Southern Ocean from nitrogen, carbon and oxygen isotopes

Thomas W. Trull[a,b,c,d,*], Diana Davies[a], Karen Casciotti[e]

[a]*Antarctic Climate and Ecosystems Cooperative Research Centre, Hobart, Australia*
[b]*Institute of Antarctic and Southern Ocean Studies, University of Tasmania, Hobart, Australia*
[c]*CSIRO Marine and Atmospheric Research, Hobart, Australia*
[d]*Laboratoire d'Etudes en Géophysiques et Océanographie Spatiales, UMR5566 (CNRS-CNES-UPS-IRD), Toulouse, France*
[e]*Department of Marine Chemistry and Geochemistry, Woods Hole Oceanographic Institution, Woods Hole, MA 02543, USA*

Accepted 16 December 2007

Abstract

The KErguelen Ocean and Plateau compared Study (KEOPS) documented enhanced iron input and phytoplankton biomass over the deep Kerguelen plateau in comparison to surrounding high-nutrient low-chlorophyll (HNLC) waters in late summer 2005. We examined the influence of this iron on nitrogen and carbon metabolism by the microbial food-web, by comparing samples from on-plateau and off-plateau. Suspended particulate organic carbon (POC) was ~5 times more abundant on-plateau and exhibited greater POC/PON (~6.5 vs. ~5.5), δ^{13}C-POC (~−21.5 vs. ~−24.5‰) and δ^{15}N-PON (~+2 vs. ~0‰) than off-plateau. These differences arose in part from changes in ecosystem structure as demonstrated by size-fractionation (1, 5, 20, 55, 210, and 335-μm filters in series), which revealed large isotopic variations with size (δ^{13}C-POC ranged from −28 to −19‰ and δ^{15}N-PON from −3 to +5‰) and greater abundances of ^{13}C- and ^{15}N-enriched large phytoplankton over the plateau. The ^{13}C enrichment in POC reflected faster growth rates and greater draw-down of dissolved inorganic carbon over the plateau. Quantitative comparison to the δ^{15}N of dissolved nitrate indicates that the δ^{15}N-PON enrichment derived from increased assimilation of nitrate, corresponding to new production *f*-ratios of 0.7–0.9 on-plateau vs. 0.4–0.6 off-plateau. Results from a sparse set of free-drifting sediment trap samples suggest control of export by zooplankton grazing. The ^{15}N and ^{18}O enrichments in dissolved nitrate exhibited a 1:1 correlation, indicating that phytoplankton assimilation controls nitrate availability and only a relatively small amount of nitrate was regenerated by nitrification. The δ^{15}N-NO_3 values yield indistinguishable isotopic fractionation factors on and off the plateau ($^{15}\varepsilon_{NO_3}$ of 4–5‰). This suggests that variations in iron availability may not bias the interpretation of paleo-environmental ^{15}N records, and leaves intact the view that higher sedimentary δ^{15}N-PON values during the last glacial maximum indicate greater fractional nitrate depletion in the Southern Ocean.

Keywords: Iron fertilization; Southern Ocean; Nitrate isotopes

1. Introduction

1.1. The influence of iron

Iron has been demonstrated to be the proximal control on Southern Ocean phytoplankton production via incubation and mesoscale iron-enrichment studies (Sedwick and DiTullio, 1997; Sedwick et al., 1999, 2002; Boyd et al., 2000; Coale et al., 2004), but the influence of iron fertilization on carbon sequestration remains unclear. Some experiments have seen enhanced export, e.g., SOFeX-south (Buesseler et al., 2005) and EIFEX (Peeken et al., 2006) while others have not, e.g., SOIREE (Nodder et al., 2001) and EisenEx (Rutgers van der Loeff and Vöge, 2001). More importantly, export responses in small-scale artificial fertilizations do not easily scale upward to explain

*Corresponding author at: AEC CRC, PB 80, University of Tasmania, Hobart 7001, Australia. Tel.: +61 3 62 262988; fax: +61 3 62 262973.
E-mail addresses: Tom.Trull@utas.edu.au, Tom.Trull@csiro.au (T.W. Trull).

0967-0645/$ - see front matter © 2008 Elsevier Ltd. All rights reserved.
doi:10.1016/j.dsr2.2007.12.035

natural iron fertilization occurring over larger regions and longer times. Persistent fertilization will alter trophic structures that influence export (Boyd and Newton, 1995; Boyd and Newton, 1999), and macro-nutrient levels that are maintained by horizontal exchange in fertilization experiments (Abraham et al., 2000; Boyd et al., 2002) may become depleted after extended exposure to iron. In particular, silicate availability may limit carbon export, because it is already almost fully consumed during its passage across the Southern Ocean from upwelled Circumpolar Deep Water in the south to its exit in mode and intermediate waters in the north (Trull et al., 2001b).

KErguelen Ocean and Plateau compared Study (KEOPS) offered the opportunity to examine primary production, ecosystem structure, and controls on export in a system accustomed, and presumably adapted, to persistent iron inputs. Nitrogen and carbon are two very useful elemental currencies in this effort to identify the ecosystem response to iron input: carbon because of its importance to atmospheric greenhouse gas budgets, and nitrogen because of its direct connection to the impact of iron on phytoplankton metabolism. Iron improves light-harvesting and many other cellular mechanisms (Geider and La Roche, 2004). In particular, the ability to use nitrate, the major form of nitrogen available in Southern Ocean surface waters, is affected by iron availability in part because nitrate reductase (the first enzyme involved in the assimilation of nitrate) requires iron (Timmermans et al., 2004).

1.2. The value of isotopic measurements

The isotopic compositions of nitrogen and carbon are useful tools with which to track the transfers and transformations of these biogeochemical currencies by ecosystem processes. They bridge the gap between the quantification offered by mass balances on relatively homogeneous dissolved nutrient fields, and the more detailed understanding of ecosystem controls on production and export offered by biological investigations. For example, comparing the carbon isotopic fractionation accompanying CO_2 draw-down in surface waters with size-fractionated phytoplankton δ^{13}C-particulate organic carbon (POC) compositions revealed that large diatoms, and not the bulk phytoplankton community, controlled export in Antarctic surface waters south of Australia (Trull and Armand, 2001). A similar comparison for nitrogen isotopes between dissolved nitrate and particulate organic nitrogen (PON) identified a switch from ammonium towards nitrate use during the SOIREE artificial iron release experiment (Karsh et al., 2003).

Combining ^{13}C and ^{15}N observations offers advantages, because these isotopes are differentially influenced by autotrophic assimilation and heterotrophic-enrichment (Fry and Sherr, 1984; Goericke et al., 1994; Altabet, 1996; Freeman, 2001; Hayes, 2001). Trophic enrichment of ^{13}C is generally small, ~1‰, while that of ^{15}N is larger, ~3.5‰. Nitrogen isotopic compositions are sensitive to the influence of regenerated nutrients, because uptake of ammonium decreases phytoplankton ^{15}N contents, in some cases by several permil (‰). In contrast, recycling of carbon to dissolved inorganic carbon (DIC) does not affect phytoplankton ^{13}C compositions, since the two carbon forms that are thought to be assimilated (CO_2 and HCO_3^-) establish chemical and isotopic equilibrium relatively quickly in the dissolved pool.

The primary control on ^{13}C contents of marine organic matter in the Southern Ocean is the isotopic composition established during photosynthesis. This process has been extensively studied and shown to depend strongly on phytoplankton size and growth rate, on whether HCO_3^- or CO_2 is assimilated (Keller and Morel, 1999; Cassar et al., 2002; Cassar et al., 2004), and on the available concentration of dissolved molecular CO_2 when it is the dominant carbon source (Laws et al., 1995; Popp et al., 1998). These so called "vital effects" impact the application of the ^{13}C composition of organic matter as a paleo-proxy for Southern Ocean carbon dioxide partial pressure (Popp et al., 1999; O'Leary et al., 2001; Lourey et al., 2004), as can secondary effects from heterotrophy and remineralization (Bentaleb et al., 1998; O'Leary et al., 2001). In contrast, PON ^{15}N contents depend primarily on the balance of ammonium and nitrate assimilation in samples dominated by phytoplankton, and on the balance of autotrophic and zooplankton contributions in bulk samples of the community (e.g., Altabet, 1996).

In localized studies, such as presented here, these biologically driven fractionations rather than variations in the isotopic compositions of the new nutrient sources (nitrate and DIC), often control the ^{15}N and ^{13}C compositions of microbial organisms. This is because the DIC source is only slightly depleted seasonally by primary production in open-ocean settings, and thus seasonal enrichment in the ^{13}C content of the DIC pool is only ~1‰. Seasonal draw-down of nitrate can cause large ^{15}N enrichments in the remaining nitrate pool in some regions (e.g., more than 5‰ over the course of the North Atlantic bloom; Altabet et al., 1991), but in the Southern Ocean the seasonal enrichment of ^{15}N in nitrate is only 1–2‰ in waters south of the Polar Front (Sigman et al., 1999b; Lourey et al., 2003; DiFiore et al., 2006).

On larger spatial scales, e.g., the progressive depletion of nitrate northward across the Southern Ocean, the enrichment of the remaining nitrate source in ^{15}N does play a role in the control of phytoplankton nitrogen isotopic compositions, and also determines the integrated isotopic composition of exported organic nitrogen over annual timescales (Francois et al., 1992; Sigman et al., 1999a; Lourey et al., 2003). This effect forms the basis of the estimation of the extent of nitrate utilization from sedimentary organic matter ^{15}N compositions (Francois et al., 1992; Sigman et al., 1999a, b; Altabet and Francois, 2001; Lourey et al., 2003), and thus evaluation of the possible role of an enhanced biological pump in the

draw-down of atmospheric CO_2 during glacial epochs (Sigman and Boyle, 2000). The quantitative scaling of ^{15}N compositions to nitrate utilization depends on the isotopic fractionation that characterizes new production, and there has been debate on whether this varies regionally in the Southern Ocean (Lourey et al., 2003; DiFiore et al., 2006), or in response to iron availability (Karsh et al., 2003).

1.3. The focus of this study

This study focuses on the impact of persistent iron fertilization on the isotopic content of the microbial ecosystem. We present measurements of the isotopic composition of dissolved nitrate (as the currency of new production), size-fractionated suspended matter from within and just below the euphotic zone (to assess uptake by phytoplankton and microbial nutrient cycling), and particles collected in free-drifting sediment traps (to examine export processes). Using these data we address three main questions:

(i) How does the enhanced iron supply over the Kerguelen Plateau affect nitrogen and carbon cycling?
(ii) Does persistent natural iron fertilization change the nitrogen isotopic fractionation that accompanies seasonal nitrate depletion, and thus affect the use of sedimentary ^{15}N as a paleo-proxy for the strength of the Southern Ocean biological pump?
(iii) What do the carbon and nitrogen isotopic compositions reveal about the ecosystem controls on carbon export?

2. Methods

2.1. Site description

The Kerguelen plateau lies to the east of Heard and the Kerguelen islands in the Indian Sector of the Southern Ocean and includes more than 45,000 km^2 of seafloor that is less than 1000 m deep (Fig. 1). As detailed by Park et al. (2008b), the plateau divides the flow of the Antarctic Circumpolar current, with the most intense flow passing to the north of Kerguelen Island in association with the Sub-Antarctic Front. Additional transport associated with the Polar Front crosses the plateau just south of Kerguelen Island, where the bathymetry reaches 600 m depth, and to the south of Heard Island via the Fawn Trough (Fig. 1). The waters around the islands and over the plateau are marked by relatively high phytoplankton concentrations in comparison to surrounding open-ocean waters (Blain et al., 2007; Mongin et al., 2008). As shown in figures in those papers, and in animation of satellite remote sensing results

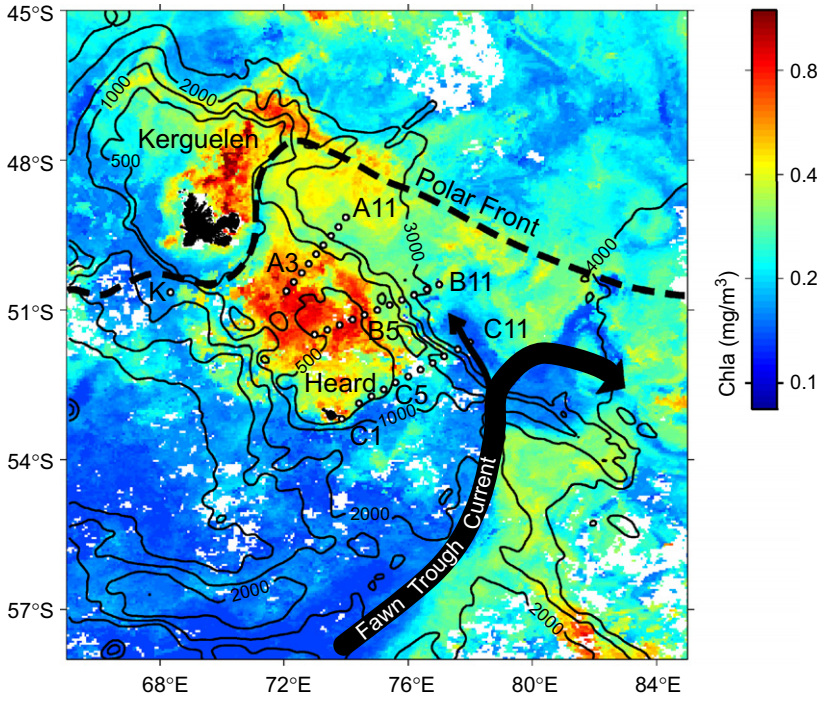

Fig. 1. Phytoplankton biomass, bathymetry, ocean circulation, and KEOPS sampling sites over the Kerguelen plateau. KEOPS carried out three transects (A, B, C) of 11 sites each. Free-drifting sediment traps were deployed once at C5 and twice at A3. Size-fractionated particles were collected at the labelled A, B, C sites. Sites A3 and B5 on the plateau exhibited the highest Chl *a* concentrations. Sites C11 and B11 off the plateau had very low Chl *a*, as did site C5 at the plateau periphery. Site A11 off the plateau had intermediate Chl *a* during KEOPS, but experienced high phytoplankton biomass at times during the 2004–05 season as revealed by satellite images (Mongin et al., 2008). Site A3 is considered to be the bloom reference station, and site C11 the HNLC reference station (Blain et al., 2007). K is the KERFIX time series site in HNLC waters to the west of the plateau (Jeandel et al., 1998). Figure adapted from Park et al. (Park et al., 2008b). Satellite chlorophyll estimates are the mean for January 2005 from the MODIS AQUA sensor (Mongin et al., 2008).

(Mongin et al., 2008), the bloom has two main features: (i) a narrow plume that extends northeast of the Kerguelen islands and north of the Polar Front that shows high mesoscale and temporal variability and (ii) a larger bloom (~45,000 km^2) south of the Polar Front, which is largely constrained to the bathymetry of the plateau. In the austral production season of 2004–2005 studied by KEOPS, this larger bloom began in early November, achieved high phytoplankton biomass (~3 μg Chl *a* l^{-1}) in December and January, and then collapsed in late February (Blain et al., 2007).

KEOPS carried out three transects across the main Kerguelen bloom in mid summer (19 January–13 February 2005) when phytoplankton abundances were rapidly decreasing (Blain et al., 2007; Mongin et al., 2008). These transects sampled waters within, at the periphery of, and outside the plateau (Fig. 1). The waters over the plateau exhibited higher biomass, greater nutrient depletion, and significant CO_2 draw-down in comparison to the surrounding high-nutrient low-chlorophyll (HNLC) waters (Blain et al., 2007; Jouandet et al., 2008; Mosseri et al., 2008). Site A3 was chosen as the reference station for the iron-fueled bloom conditions (Blain et al., 2007), based on high phytoplankton biomass (Chl *a* of 1.1–2.1 μg L^{-1} between 0 and 125 m) and lowered $Si(OH)_4$ concentrations in surface water (1.8 μM), but still elevated NO_3^- (23.0 μM; Mosseri et al., 2008). Site C11 was designated as the corresponding reference station for off-plateau HNLC conditions (0.1–0.2 μg L^{-1} Chl *a*, 25.1 μM $Si(OH)_4$, and 29.4 μM NO_3^-). Surface dissolved iron levels were low at all stations, but sub-surface levels and hence supply of iron to surface waters was elevated over the plateau (Blain et al., 2007, 2008). Carbon export over the plateau was approximately twice that of surrounding waters, as estimated from ^{234}Th distributions (Blain et al., 2007; Savoye et al., 2008).

Phytoplankton communities at all the sites were dominated by common Southern Ocean diatoms but with differences in the relative abundances of species at the on-plateau and off-plateau stations (Armand et al., 2008). Much of this biomass consisted of large diatoms and diatom chains, with more than 80% of the biogenic silica in the >10 μm size class at A3, and more than 70% at C11 (Mosseri et al., 2008). More and larger zooplankton were present on-plateau than off-plateau (Carlotti et al., 2008), and bacterial populations were larger and more active (Obernosterer et al., 2008). Additional details of the ecosystem structure of the Kerguelen bloom and the surrounding waters are presented in the discussion below (and in the accompanying papers in this issue).

2.2. Sampling

Three types of samples were collected for nitrogen and carbon isotopic study: (i) seawater from Niskin bottles deployed on the CTD rosette for isotopic compositions of dissolved nitrate, (ii) size-fractionated suspended particles using a large-volume pump, and (iii) sinking particles from short-term deployments of a free-drifting sediment trap. The locations of these collections are shown in Fig. 1.

Sampling on-plateau focused on sites A3 (the bloom reference station) and B5 at the centre of the plateau, and C5 at its southeastern edge. Sampling off-plateau focused on the eastern end of the three transects at sites A11, B11, and C11 (the HNLC reference station). The other stations exhibited either similar properties to these reference stations end-members (with B5 similar to A3, and B11 similar to C11) or intermediate properties (C5 at the plateau edge had relatively low biomass in comparison to other plateau stations, and Station A11 off the plateau to the northeast had relatively high biomass in comparison to other HNLC stations; Mosseri et al., 2008; Armand et al., 2008). These intermediate conditions appear to reflect the circulation around the plateau, which brings HNLC waters onto the plateau from the south and west, and sweeps it off the plateau to the north and east (Park et al., 2008b). The two on-plateau bloom stations also differed in the detailed timing of biomass accumulation. The reference site A3 exhibited steadily declining biomass during the KEOPS survey, in keeping with the overall late summer decline of the bloom (Blain et al., 2007), but station B5 experienced an increase in biomass late in the KEOPS survey period as seen in satellite ocean-colour images (Mongin et al., 2008).

Suspended particles were collected from four depths (~20, 60, 100, and 130 m) within and just below the euphotic zone using an *in-situ* impeller pump which returns water to the deck via a hose (Trull and Armand, 2001). On deck, the water passed through a cascade of filters: first a 47-mm diameter 1000-μm pre-screen to remove large zooplankton, followed by 142-mm diameter nylon screens (335, 210, 55, 20, and 5-μm mesh sizes) and a final 142-mm diameter QMA quartz fibre filter (1 μm nominal pore size). The quartz filter was used in preference to GF/F glass fibre filters to minimize ^{234}Th backgrounds. Previous work with this pump suggests that it does not significantly damage phytoplankton cells, in that intact chains of pennate diatoms are recovered (Trull and Armand, 2001) and fast repetition rate fluorometric parameters of samples collected with the pump are indistinguishable from samples collected in Niskin bottles (F.B. Griffiths and T. Trull, unpublished results). The flow path allowed a larger flow rate through the larger meshes, so that during the ~1 h of filtration at each depth, 50–150 L passed through the QMA filter at ~1–3 L per minute while 200–600 L passed through the 335- and 210-μm meshes. At most, a few large euphausids were obtained on the pre-screen and this material was not analysed.

The particles on the other screens were immediately resuspended (in 1-μm filtered seawater from the sampling depth) and refiltered onto 25-mm diameter, 1.2-μm pore size silver membrane filters and, along with the QMA filter, were dried at 60 °C for shipboard ^{234}Th analysis, followed by carbon and nitrogen analyses in the laboratory in Hobart. At some stations, the QMA filter began to clog after 30–45 min and it was removed from the flow path.

At the A3 site, the size distribution of particles was focused strongly on the 55-μm screen, and this also began to limit flow during the collection period, and for this station that fraction may include some smaller particles.

Sinking particles were collected with a cylindrical sediment trap (with a 0.125-m^2 collection area and an internal conical funnel that transfers the sinking particles to a carousel of collection cups, model PPS3/3, Technicap Inc., France) suspended at 200 m depth beneath a free-drifting surface float equipped with an ARGOS beacon and a strobe light. Following loss of other traps during earlier deployments at A3 and C11, this trap was successfully deployed 3 times (twice at A3—designated A3i and A3f for initial and final, and once at C5, Fig. 1), and thus provides only a small set of observations. On each occasion the trap was deployed for ~24 h and drifted a relatively small distance (~10 km) in comparison to the dimensions of the studied features. Further details of the deployment dates and trap drifts are provided in (Ebersbach and Trull, 2008). Four cups filled with trace-metal clean brine (salinity ~60 prepared by freezing sub-surface seawater) but no poison because of the short deployments in cold water were rotated beneath the funnel during each deployment. Two of these were used for trace-metal studies (Bowie et al., in preparation) and two were used for the nitrogen and carbon isotopic analyses reported here.

On recovery, the cup solutions were filtered through a 350 μm nylon mesh to separate zooplankton "swimmers". The materials on this mesh were vigorously sprayed with seawater (pre-filtered through a 1 μm quartz filter) to disperse faecal pellets and wash them and any material clinging to the copepods through the mesh. Both the >350- and <350-μm size fractions were resuspended (in 1-μm filtered seawater) and refiltered onto 25-mm, 1.2-μm silver filters. These samples were dried and analysed following the same procedures as for the suspended particles. Examination by onboard microscopy revealed few swimmers in the <350-μm size fractions, and no additional separation was attempted.

Seawater samples for dissolved nitrate $\delta^{15}N$ and $\delta^{18}O$ analyses were collected from Niskin bottles attached to the CTD-Rosette to provide vertical profiles in the top 200 m twice at site A3 (A3i and A3f) and once at site C11. Samples from the mixed layer were also collected from other sites (Table 1). Seawater was transferred directly from the Niskin bottles to acid-leached 250-ml polypropylene bottles and frozen at −20 °C until thawed for isotopic analysis in the Woods Hole laboratory.

2.3. Analyses

The filters with the suspended and sinking particles were examined under stereo-microscopy onboard the ship at magnification up to 50×. The largest size-fractions (>350 μm for the sinking particles and 335–1000-μm fractions for the suspended particles) were dominated by zooplankton, primarily copepods. Intact faecal pellets did not contribute significantly to these fractions. For the sinking particles this is because they were deliberately dispersed and washed through the 350-μm screen used to separate swimmers from the sinking flux. For the suspended particles this is presumably the result of dispersion of faecal pellets and other aggregates during the passage of the water through the impeller pump, hose, and filtration system, because large faecal pellets and aggregates of faecal pellets were observed in sediment traps equipped with polyacrylamide gels (Ebersbach and Trull, 2008).

The smaller size-fractions were dominated by diatom frustules, with small centric diatoms abundant on the 5-μm filter, a mix of centric and pennate diatoms on the 20- and 55-μm filters, and large diatoms and chains of pennate diatoms and small copepods on the 210-μm filter. The particles on the 1-μm quartz filter were too small to examine in any detail using stereo-microscopy. The light beige colour of these filters, in comparison to the greener shades of the intermediate sizes, suggests contributions from detritus and/or bacteria. More detailed information on the organisms present on our filters is not available, but other studies of bacterial abundances (Obernosterer et al., 2008), phytoplankton pigments (Griffiths and Uitz, 2006), diatom species (Armand et al., 2008), and zooplankton net tows (Carlotti et al., 2008) are consistent with our overall interpretation that the size-fractionated samples are dominated by detritus and bacteria (1-μm filter), diatoms (5, 20, and 55-μm screens), a mix of diatoms and copepods (210-μm screen) and copepods (335-μm screen).

The POC, PON, $\delta^{13}C$-POC, and $\delta^{15}N$-PON analyses were carried out in Hobart. Sub-samples of the 25-mm diameter silver membrane filters were placed in acid-resistant silver cups, treated with two 10-μl aliquots of 2N HCl (and 2×20 μl for the QMA filters) to remove carbonates (King et al., 1998), and dried at 60 °C. A first set of sub-samples was analysed for POC and PON concentrations by combustion of the silver cups in a Thermo-Finnigan Flash 1112 elemental analyser with reference to sulphanilamide standards in the Central Sciences Laboratory of the University of Tasmania. Precision of the analyses was ~1%, but the overall precision was limited to 5–10% by the sub-sampling of the filters. Based on the POC and PON results, a second set of sub-samples was punched for the isotopic analyses.

$\delta^{13}C$-POC and $\delta^{15}N$-PON were analysed separately using a Fisons 1500 Elemental Analyser coupled via a Con-flow II interface to a Finnigan Delta^{PLUS} isotope ratio mass spectrometer at CSIRO Marine and Atmospheric Research. During the ^{15}N analyses, CO_2 was removed using a sodium hydroxide scrubber (self-indicating Ascarite 2, Thomas Scientific) to avoid CO^+ interference at m/z 29 and 28 (Brooks et al., 2003). Small-bore combustion and reduction columns were used to increase sensitivity, which ensured signals in the mass spectrometer of at least 1 V (and generally >2 V). With these modifications, analysis of as little as 5 μg-N was possible, but the optimal range was 15–50 μg-N, and filters were sub-sampled accordingly.

Table 1
$\delta^{15}N$ and $\delta^{18}O$ compositions of dissolved nitrate

Site	Date	Depth (dbar)	NO_3 (μM)	n^a	$\delta^{18}O$-NO_3 mean	$\delta^{18}O$-NO_3 $1\sigma^b$	$\delta^{15}N$-NO_3 mean	$\delta^{15}N$-NO_3 $1\sigma^b$
A03	19/1/05	41.1	21.2	2	5.16	0.30	6.81	0.23
A03		21.5	20.8	2	5.16	0.30	6.85	0.24
A11	20/1/05	40.9	22.5	2	4.84	0.30	6.73	0.27
A11		20.8	22.5	2	4.93	0.30	6.77	0.40
A01	23/1/05	40.8	21.3	2	4.92	0.30	6.82	0.20
A01		20.4	21.4	2	5.08	0.30	6.96	0.20
A3i	23/1/05	251.9	30.1	3	3.18	0.30	5.37	0.20
A3i		202.0	28.8	3	3.31	0.42	5.17	0.22
A3i		179.8	27.8	3	3.57	0.47	5.43	0.20
A3i		162.4	26.7	3	4.09	0.51	5.62	0.20
A3i		141.0	22.8	3	4.74	0.31	6.44	0.21
A3i		132.8	22.4	3	4.63	0.50	6.46	0.20
A3i		121.0	21.8	3	4.80	0.45	6.59	0.20
A3i		111.3	21.4	3	4.72	0.35	6.75	0.27
A3i		101.8	21.0	3	4.85	0.47	6.78	0.20
A3i		50.9	20.5	3	5.18	0.30	7.10	0.20
A3i		24.8	20.1	3	5.16	0.30	7.17	0.20
A3i		5.8	20.6	3	5.02	0.30	7.04	0.20
C11	28/1/05	253.5	33.1	2	2.39	0.30	5.20	0.20
C11		201.3	31.3	2	2.73	0.30	5.29	0.20
C11		182.0	30.7	3	2.99	0.30	5.35	0.20
C11		159.9	28.9	3	3.27	0.35	5.47	0.20
C11		141.5	28.6	3	3.23	0.30	5.71	0.20
C11		130.5	27.8	3	3.22	0.30	5.75	0.20
C11		112.2	27.1	3	3.39	0.30	6.00	0.20
C11		101.6	26.5	3	3.50	0.30	6.11	0.20
C11		48.6	26.2	3	3.56	0.32	6.20	0.20
C11		20.1	26.5	3	3.67	0.30	6.25	0.20
C11		6.2	26.5	3	3.49	0.30	6.19	0.20
B11	29/1/05	19.7	26.2	2	3.67	0.30	6.25	0.35
B05	1/2/05	20.5	22.4	2	4.60	0.30	6.74	0.20
B01	2/2/05	21.1	22.8	2	4.65	0.30	6.71	0.20
C05	7/2/05	29.7	22.0	2	3.86	0.30	6.28	0.20
C01	9/2/05	18.9	21.9	2	3.72	0.30	5.85	0.20
Kerfix	10/2/05	20.0	24.9	2	4.24	0.30	6.50	0.20
A3f	12/2/05	201.2	24.9	2	3.16	0.30	5.29	0.20
A3f		141.0	23.8	2	3.64	0.30	5.18	0.30
A3f		131.9	23.5	2	3.66	0.30	5.65	0.20
A3f		120.5	24.5	2	4.09	0.30	5.88	0.20
A3f		111.0	24.4	2	4.11	0.30	6.12	0.20
A3f		101.2	29.9	2	4.30	0.30	6.39	0.20
A3f		90.3	28.9	2	4.59	0.30	6.64	0.20
A3f		40.1	26.8	2	4.71	0.30	6.74	0.24
A3f		19.7	25.4	3	4.84	0.30	6.68	0.24
A3f		10.8	25.1	3	4.84	0.30	6.75	0.31

[a] n = number of replicate of the isotopic compositions.
[b] Minimum 1σ were set to 0.30‰ for $\delta^{18}O$-NO_3 and 0.20‰ for $\delta^{15}N$-NO_3.

The $\delta^{15}N$ and $\delta^{13}C$ isotopic compositions are expressed in delta notation vs. atmospheric N_2 and the VPDB standard, respectively. Standardization was by reference to CO_2 and N_2 working gases injected before and after each sample, with normalization to two solid reference materials run (along with blank cups) after each six samples. For $\delta^{13}C$, the solid standards were NBS-22 oil (RM8539, −29.73‰) and NBS-19 (limestone, RM8544, +1.95‰). For $\delta^{15}N$, the solid standards were IAEA-N1 (ammonium sulphate, RM8547, +0.4‰) and IAEA-N3 (potassium nitrate, RM8549, +4.7‰). Based on replicate analyses of these standards the estimated precisions were typically 0.1‰ for 1 standard deviation for both $\delta^{13}C$ ($n = 15$) and $\delta^{15}N$ ($n = 20$). Sample replicates generally had comparable precisions to the reference materials, but filters with patchy coverage had lower precision (0.3‰ in the worst cases, presumably reflecting isotopic heterogeneity within the size fractions). Procedural blanks were measured by passing 1 L of seawater through the onboard pumping system and subsequent processing in parallel to the samples, and yielded negligible amounts of POC and PON (<1% of typical samples), and with ratios close to those of the samples, and no correction was applied.

The N and O isotopic compositions of nitrate were measured by converting dissolved nitrate (and small amounts of nitrite, present at less than 1% of the nitrate in these samples) to N_2O using the denitrifier method with *Pseudomonas aureofaciens* (Sigman et al., 2001; Casciotti et al., 2002). Analysis was done with a Finnigan Delta^{PLUS} XP mass spectrometer at WHOI. Replicates of each sample were analysed on separate days ($n = 2$ or 3), with sample volumes adjusted to achieve 20 nmols NO_3^- per analysis (0.6–1.1 ml seawater). The standard deviations shown in Table 1 are based on these replicate analyses, with the caveat that minimum uncertainties were set to 0.3 for $\delta^{18}O$ and 0.2 for $\delta^{15}N$, so that replicates that fell very close together by chance did not over-represent the precision of the results.

Calibration of $\delta^{15}N$ and $\delta^{18}O$ for the nitrate samples was via parallel analyses of two standards (USGS32 with $\delta^{15}N = +180‰$ and USGS34 with $\delta^{15}N = -1.8‰$), (Bohlke et al., 2003) to place the $^{15}N/^{14}N$ ratios on the AIR reference scale, and three standards (USGS32 with $\delta^{18}O = +25.7‰$, USGS34 with $\delta^{18}O = -27.9‰$, and USGS35 with $\delta^{18}O = +57.5‰$), (Bohlke et al., 2003) to place the $^{18}O/^{16}O$ ratios on the VSMOW reference scale. This multiple-standard calibration technique has been described previously (Casciotti et al., 2002), although at that time well-calibrated standards were not available for its application. An aliquot of each reference material was analysed at the beginning of each batch of samples and after every nine samples to obtain six replicates of each standard in a typical run of 45 samples, thereby providing precise regressions for the multiple-standard calibration procedure, as well as minor corrections based on linear temporal drift. The new standard values as applied here lead to $\delta^{18}O$ values that are approximately 2.9‰ higher than those based on earlier estimates for these standards (for recent discussion see Sigman et al., 2005).

Nitrate and nitrite were measured onboard the R.V. *Marion Dufresne* using University of Marseille methods as adapted from (Tréguer and LeCorre, 1975). This method measures the sum of nitrate and nitrite, rather than nitrate directly, but results for nitrite from a subset of the samples showed that it represented $<1\%$ of the total nitrate + nitrite, and thus results for nitrate + nitrite result have been taken to represent nitrate alone for the purposes of estimating isotopic fraction associated with nitrate depletion. Because shipboard analyses were not always available for the same Niskin bottles as sampled for ^{15}N-NO_3, dissolved nitrate concentrations also were measured at CSIRO Marine and Atmospheric Research using a Lachat flow-injection auto-analyser (and the manufacturer's QuickChem methodology) on separate samples taken from the same Niskin bottles sampled for ^{15}N-NO_3 (originally collected for ^{13}C-DIC analyses and poisoned with mercuric chloride and stored tightly sealed at room temperature). These results agree to within $\sim 1\,\mu M$ with the more extensive shipboard results for most but not all samples (not shown). Because of the strong nitrate gradients in the seasonal pycnocline (Fig. 2A) and thus the desirability of having both concentration and isotopic measurements from the same Niskin bottles, we have used only the CSIRO results for the calculation of isotopic fractionation factors, but also refer to the shipboard results for broader context.

3. Results and discussion

3.1. Nitrogen isotopic composition of dissolved nitrate: negligible influence of iron on isotopic fractionation accompanying nitrate depletion

The three nitrate profiles (A3i, A3f, and C11) exhibited partial nitrate draw-down above the summer pycnocline from seasonal assimilation and export (~30% of remnant winter water values at the sub-surface temperature minimum, Fig. 2A), with greater nitrate depletion at the on-plateau bloom site (A3) than the off-plateau HNLC site (C11). In concert with this nitrate draw-down, $\delta^{15}N$-NO_3 increased to ~6‰ off the plateau at the HNLC reference station C11 and ~7‰ on the plateau in the centre of the bloom at station A3 (Fig. 2B), with intermediate values in surface waters at other sites (Table 1). $\delta^{15}N$-NO_3 values below 200 m were similar on and off-plateau at ~5.25‰, and close to global deep-ocean average values of ~5‰ (Sigman et al., 2000, 2005).

Assuming that photosynthetic nitrate assimilation is the only process that removes nitrate and that nitrate resupply is negligible, the $\delta^{15}N$-NO_3 results should show a Rayleigh distillation relation, i.e. they should reflect closed system evolution so that $\delta^{15}N$-NO_3 correlates linearly with the logarithm of the nitrate concentrations with a slope equal to the isotope effect ($^{15}\varepsilon_{NO_3}$) of nitrate removal (Sigman et al., 1999b). The three profiles do display linear relations (Fig. 2D) and yield indistinguishable estimates of $^{15}\varepsilon_{NO_3}$ (Table 2) that are very similar to the values of 4–5‰ estimated for Polar Frontal Zone and Antarctic surface waters from transects (Sigman et al., 1999b). However, these estimates of $^{15}\varepsilon_{NO_3}$ fall well below the values (~8–9‰) estimated from profiles in southern Antarctic Zone waters during the SOIREE project (Karsh et al., 2003) and from profiles in Sub-Antarctic waters (DiFiore et al., 2006). This variability appears to be a real characteristic driven by ecosystem differences (DiFiore et al., 2006).

Estimating $^{15}\varepsilon_{NO_3}$ in this way is, of course, dependent on the closed system assumption and the hypothesis of the applicability of a single $^{15}\varepsilon_{NO_3}$. Physical resupply of nitrate across the seasonal pycnocline or horizontally from surface waters with higher nitrate concentrations is likely to occur and tends to lead to under-estimates of $^{15}\varepsilon_{NO_3}$ of the order of 1‰ for the relatively low extent of nitrate depletion in the Southern Ocean (Sigman et al., 1999b). It is possible that the slightly lower $^{15}\varepsilon_{NO_3}$ value obtained for the A3f profile (Table 2) has arisen in this way. This profile was collected during the passage of a large internal wave that

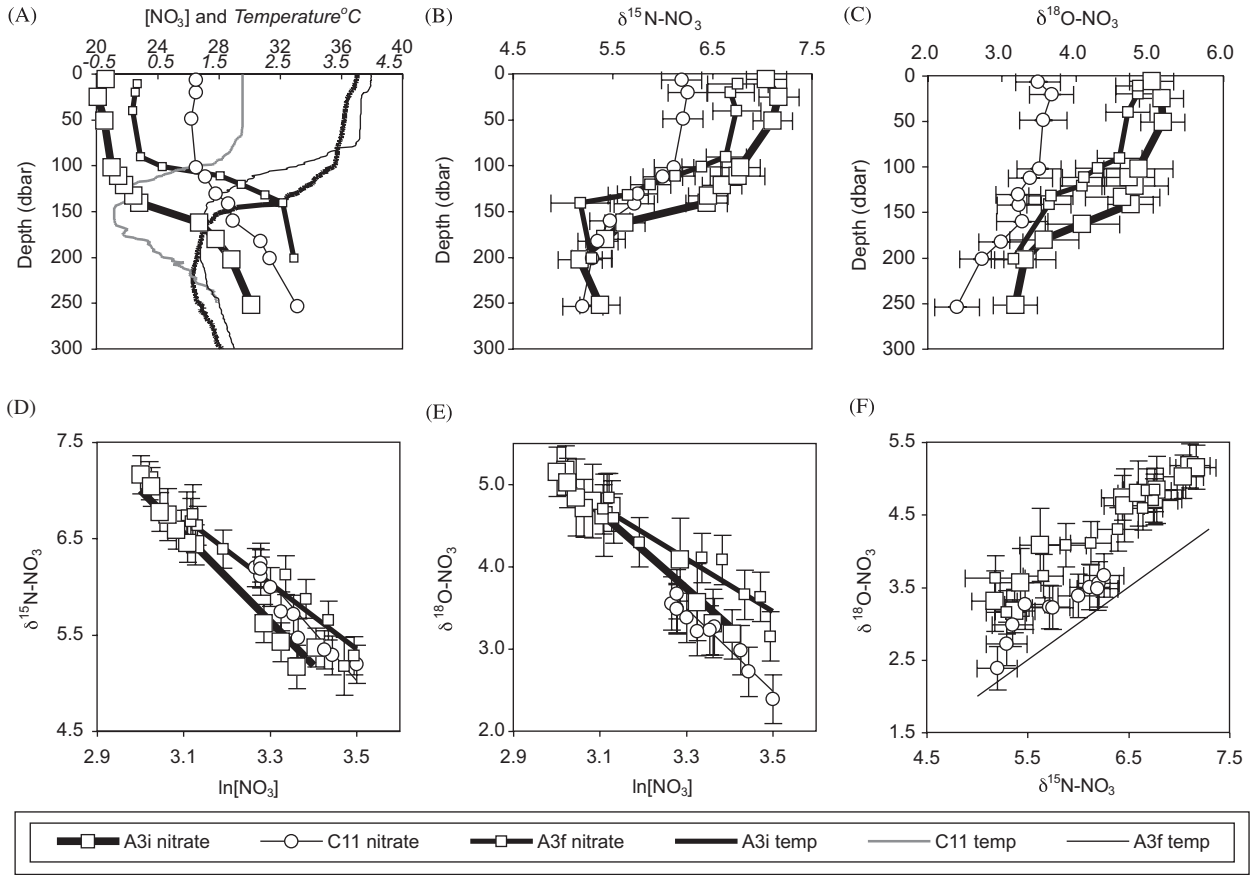

Fig. 2. Dissolved nitrate concentrations and isotopic compositions: (A) nitrate and potential temperature profiles, (B) δ^{15}N-NO_3 (‰ vs. AIR) profiles, (C) δ^{18}O-NO_3 (‰ vs. VSMOW) profiles, (D) δ^{15}N-NO_3 Rayleigh diagram, (E) δ^{18}O-NO_3 Rayleigh diagram, and (F) δ^{18}O-NO_3 vs. δ^{15}N-NO_3, with line indicating 1:1 correlation through mean deep seawater (see Section 3.2).

Table 2
Closed system (Rayleigh) isotopic fractionation factors

Site	n[a]	$^{15}\varepsilon_{NO_3}$	±1s.d.	$\lvert r\rvert$	$^{18}\varepsilon_{NO_3}$	±1s.d.	$\lvert r\rvert$
A3i	12	−4.55	0.39	0.981	−4.63	0.69	0.985
A3f	10	−3.41	0.45	0.985	−3.19	0.59	0.949
C11	11	−5.13	0.92	0.886	−4.99	1.39	0.887

[a] n = number of samples in profile.

lifted the isotherms in the upper water column (Fig. 2A), and these waves enhanced vertical mixing during KEOPS (Park et al., 2008a).

Resupply of nitrate by bacterial nitrification would also cause departure from the Rayleigh model, potentially leading to underestimated $^{15}\varepsilon_{NO_3}$ (Sigman et al., 1999b). In general, ammonium assimilation by phytoplankton is expected to greatly out-compete nitrification as a sink for ammonium in surface waters because of light inhibition of nitrifying bacteria (Olson, 1981), but shipboard nitrification measurements in the open ocean west of the Kerguelen plateau found that nitrification and assimilation contributed approximately equally to ammonium consumption in surface waters (Bianchi et al., 1997). Similar incubations with ^{15}N-enriched ammonium during KEOPS suggest that surface mixed-layer nitrification rates were less than 10% and often less than 5% of ammonium uptake rates over the plateau, although nitrification rates reached and sometimes exceeded phytoplankton ammonium assimilation rates in waters within and below the seasonal pycnocline (P. Raimbault, Université de Marseille, personal communication). The absolute rates of nitrification measured during KEOPS could resupply less than 10% of the seasonal depletion of nitrate observed in surface waters, implying that most of the nitrate could be considered as "new" for the purposes of a seasonal Rayleigh uptake model. In combination, the effects of physical resupply and nitrification suggest that our closed system estimates of $^{15}\varepsilon_{NO_3}$ are likely to be low by ~1‰. In keeping with other Southern Ocean studies (Sigman et al., 1999b; Lourey et al., 2003; Karsh et al., 2003; DiFiore et al., 2006), we acknowledge but have not corrected our estimates for this bias.

The similarity of the $^{15}\varepsilon_{NO_3}$ estimates on and off the plateau argues against a response of isotopic fractionation to the availability of iron. This suggests that the apparent decrease in $^{15}\varepsilon_{NO_3}$ during the SOIREE artificial iron fertilization, which was deduced from reduction in the offset between δ^{15}N-NO_3 and δ^{15}N-PON (Karsh et al.,

2003), may have been the result of a switch from ammonium to nitrate use by the phytoplankton community, rather than a real change in $^{15}\varepsilon_{NO_3}$. This possibility was discussed by Karsh et al. (2003), but their data could not resolve the issue. This is good news for the interpretation of paleo-environmental ^{15}N records and leaves intact the general conclusion that higher sedimentary δ^{15}N-PON values during the last glacial maximum indicate greater fractional nitrate depletion in the Southern Ocean (Francois et al., 1992; Sigman et al., 1999a; Sigman and Boyle, 2000). However, the quantitative scaling of the isotopic composition to nitrate consumption depends on many variables that are not yet well known and appear to vary regionally (Karsh et al., 2003; Lourey et al., 2004; DiFiore et al., 2006). Attention to other possible causes of variations in δ^{15}N- PON and $^{15}\varepsilon_{NO_3}$ is of course still necessary in the quantitative interpretation of the sedimentary δ^{15}N-PON variations (Francois et al., 1992, 1997; Altabet and Francois, 1994; Sigman et al., 1999a, b; Sigman and Boyle, 2000; Karsh et al., 2003).

3.2. Oxygen isotopic composition of dissolved nitrate: a small role for local nitrification in nitrogen cycling

The denitrifier method allows the determination of the oxygen as well as the nitrogen isotopic composition of nitrate (Casciotti et al., 2002). Differences in the extent of isotopic fraction of these two elements can provide information on the role of nitrification and denitrification in controlling nitrate concentrations (Casciotti et al., 2002; Sigman et al., 2005) and in examining inputs of new N from nitrogen fixation (Sigman et al., 2005).

The δ^{18}O-NO_3 of our deepest samples, which represent the first estimates for the Southern Ocean, were similar to those of deep ocean nitrate elsewhere in the global ocean (Casciotti et al., 2002; Sigman et al., 2005) and more extensive preliminary results from the Southern Ocean (P. DiFiore, personal communication) after inclusion of the calibration scale offset for our δ^{18}O calibration relative to earlier work (see Section 2). The general shape of δ^{18}O-NO_3 profiles were similar to those of δ^{15}N-NO_3 (Figs. 2B and C) and yield similar values for $^{18}\varepsilon_{NO_3}$ from their Rayleigh slopes on and off the plateau (Fig. 2E) that are subject to similar biases and caveats as discussed for $^{15}\varepsilon_{NO_3}$ above.

Nitrate assimilation by phytoplankton produces a approximately 1:1 correlation in the residual δ^{18}O-NO_3 and δ^{15}N-NO_3 isotopic compositions (Casciotti et al., 2002; Granger et al., 2004), but higher δ^{18}O-NO_3 at a given δ^{15}N-NO_3 can occur if reduced nitrogen (PON, DON, ammonia, etc.) is returned to the nitrate pool by nitrification (Casciotti et al., 2002; Sigman et al., 2005). In our profiles, the variations in δ^{18}O-NO_3 and δ^{15}N-NO_3 are close to the 1:1 correlation line expected to result from nitrate assimilation alone (Fig. 2F), as expected from more extensive studies of the Southern Ocean (DiFiore et al., 2006). However, the overall results plot consistently above the correlation expected for 1:1 enrichment from a mean deep-ocean source (δ^{18}O-NO_3 ~2.0‰, and δ^{15}N-NO_3 ~5.0‰ on our calibration scale). In addition, for a given δ^{15}N-NO_3 value the δ^{18}O-NO_3 profiles are ~0.5‰ higher over the plateau at A3 than off-plateau at C11. The origin of this enrichment in δ^{18}O-NO_3 is uncertain, but suggests the possibility of a secondary contribution from nitrification (Casciotti et al., 2002; Sigman et al., 2005) resulting from a greater rate of remineralization and recycling of nitrate over the plateau.

A small contribution from nitrification is in keeping with the absolute rates of nitrification of the order of 10 nM d^{-1} observed in shipboard ^{15}N-enriched ammonium incubations during KEOPS, as mentioned above (Raimbault et al., in preparation). At these rates ~1 μM nitrate is produced over the ~90-day period of the Kerguelen bloom, which is a small fraction of the seasonal nitrate depletion of ~8 μM in surface waters (Fig. 2A). Applying a calculation similar to that of Sigman et al. (2005) and assuming that nitrification adds nitrate with δ^{18}O close to local δ^{18}O-H_2O values (Meredith et al., 1999) suggest that a few cycles of ~30% fractional consumption of nitrate by phytoplankton followed by remineralization and nitrification would be required to increase the δ^{18}O-NO_3 over the plateau by ~0.8‰ relative to δ^{15}N-NO_3. Thus, to achieve the higher δ^{18}O-NO_3 values over the plateau via nitrification in the water column would require multi-year residence times of water over the plateau, but this appears unlikely based on circulation studies (Park et al., 2008b). Alternatively, the δ^{18}O-NO_3 offset between the on-plateau and off-plateau results may represent differences related to the isotopic composition of the initial nitrate supply-which is derived from further south at the off-plateau station (C11) than at the on-plateau station (Park et al., 2008b). Evaluation of that possibility will require the development of more extensive δ^{18}O-NO_3 observations in the Southern Ocean.

3.3. Bulk particle compositions: large differences between on- and off-plateau samples

The bulk (i.e. summed over all size fractions) particulate C and N concentrations and isotopic compositions are notable for their large variations (Fig. 3; Table 3). The on-plateau high-biomass sites (A3 and B5) are distinguishable from the off-plateau low-biomass sites (B11 and C11) in having generally higher POC concentrations, higher POC/PON ratios (except B5), higher δ^{15}N-PON, and higher δ^{13}C-POC. The moderate-biomass off-plateau site to the east of the bloom (A11), and the low-biomass site at the southern edge of the plateau (C5) display intermediate compositions consistent with their intermediate oceanographic contexts (see Section 2.2).

The overall ranges of these concentrations and isotopic compositions were generally similar to previous studies. The POC concentrations ranged from less than 1 to nearly 10 μM consistent with previous Southern Ocean

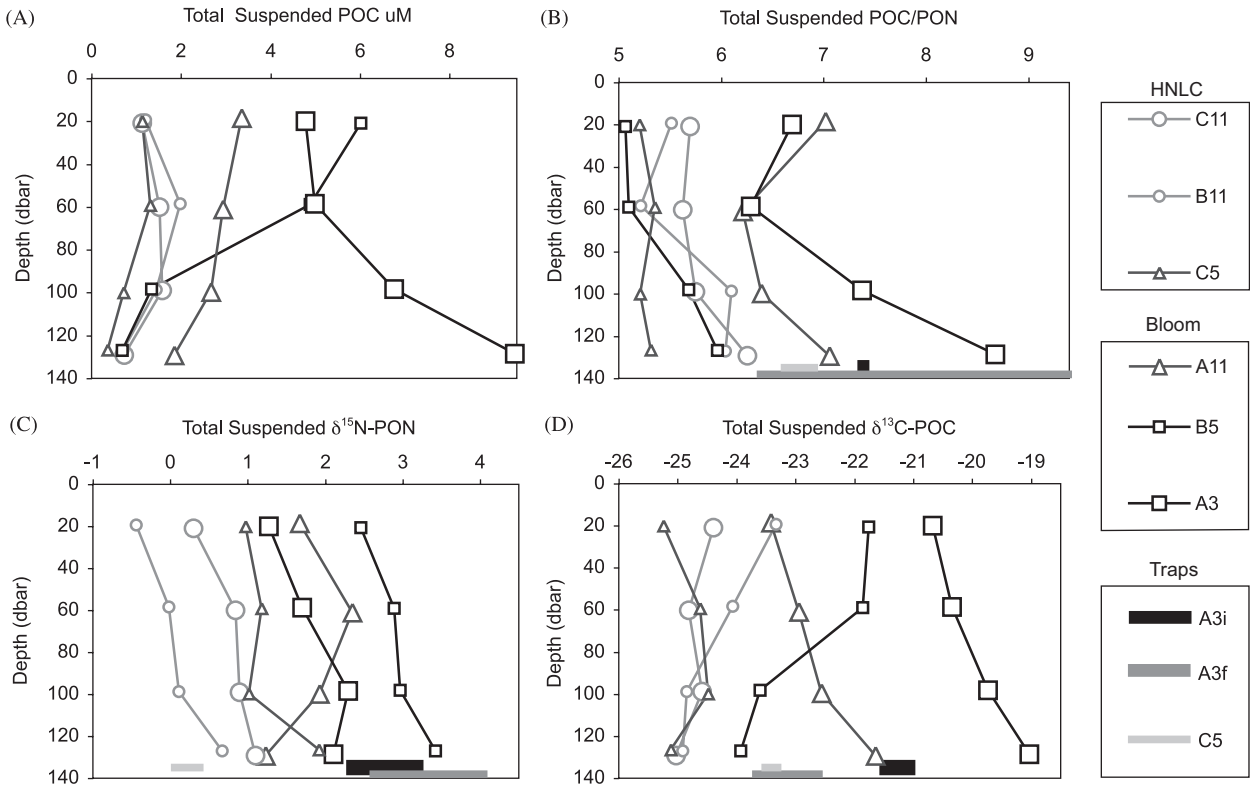

Fig. 3. Vertical profiles of total suspended particles and sediment trap sample compositions: (A) POC (μM), (B) POC/PON, (C) δ^{15}N-PON (‰ vs. AIR), (D) δ^{13}C-POC (‰ vs. VPDB). Horizontal bars below the profiles indicate sediment trap particles collected once at site C5 and twice at A3 (see Table 5).

surveys that transited HNLC and bloom conditions (Copin-Montegut and Copin-Montegut, 1983; Lourey and Trull, 2001). The POC/PON ratios ranged from 5 to 6 (except at A3 and A11 where higher values were observed-as discussed below). This is lower than the Redfield ratio (6.6) for average phytoplankton, but similar to results from these previous Southern Ocean studies for particulate organic matter. δ^{15}N-PON ranged from less than 0‰ at the off-plateau HNLC sites to more than 2‰ at the on-plateau bloom sites (Fig. 3C), similar to values seen in the Sub-Antarctic Zone south of Tasmania in summer, but not as low as values of −2‰ to −5‰ in the Polar Frontal Zone that have been attributed to the influence of ammonium recycling (Lourey et al., 2003). δ^{13}C-POC ranged from less than −25‰ to more than −20‰ (Fig. 3D), similar to variations across the Southern Ocean from the Sub-Antarctic Zone south across the Polar Front and into ice-free Antarctic surface waters south of Australia (Popp et al., 1999; Trull and Armand, 2001; Lourey et al., 2004) and from the Subtropical Convergence south to Kerguelen Island (Bentaleb et al., 1998).

All of the stations show decreasing POC concentrations with depth (Fig. 3A), with the exception of the A3 bloom reference station where POC increased with depth, as was also observed for particulate biogenic silica and for Chl *a* at this station (Mosseri et al., 2008). This feature was particularly prominent early in the KEOPS study, but also occurred at later reoccupations of the A3 site and at adjacent stations to the east and west along the A transect, and may reflect settling of the increasingly senescent diatom bloom over the plateau (Mosseri et al., 2008). Bulk POC/PON ratios generally increased with depth by 0.5, except at A3 where a stronger increase occurred (Fig. 3B). Bulk δ^{15}N-PON increased ~0.5‰ with depth at all stations except A11 (Fig. 3C). Bulk δ^{13}C-POC exhibited both decreases and increases with depth (Fig. 3D). The POC/PON and δ^{15}N-PON increases appear to reflect preferential recycling of nitrogen vs. carbon, although the story is more complex and includes changes in particle size distributions (which also affect the δ^{13}C-POC variations), as discussed in more detail below.

3.4. *Size-fractionated suspended particle POC and PON concentrations: iron-induced increases in the autotrophic contribution*

The compositional differences between the on-plateau and off-plateau sites reflect a combination of changes in the microbial ecosystem as reflected in the size class structure, and with changes in physiological and nutritional processes. The distribution of POC across the six size fractions varies systematically between the off-plateau and the on-plateau stations. The off-plateau HNLC stations C11 and B11 (and to a lesser extent the HNLC station C5 at the plateau periphery) have most of their POC in the larger size fractions, with maximal contributions from either the 210- or 335-μm fractions (Fig. 4A). In contrast, the on-plateau

Table 3
δ^{15}N and δ^{13}C compositions of size-fractionated suspended particles

		Size-fraction (μm)	POC (μM)	POC/PON atom	δ^{13}C-POC ‰PDB	δ^{15}N-PON ‰AIR			Size-fraction (μm)	POC (μM)	POC/PON atom	δ^{13}C-POC ‰PDB	δ^{15}N-PON ‰AIR
Site	A11	335	0.32	4.8	−23.11	2.80	Site	B5	335	0.88	4.7	−21.87	2.35
date	20/1/05	210	0.43	5.4	−24.63	2.57	date	31/1/05	210	0.91	4.5	−22.65	3.09
depth	18.3±0.8	55	0.76	8.0	−24.04	2.05	depth	20.7±1.2	55	2.07	5.1	−21.86	2.42
		20	0.81	8.7	−22.78	1.97			20	1.77	5.4	−20.86	2.51
		5	0.78	6.8	−22.26	0.40			5	0.25	5.8	−21.95	1.06
		1	0.24	9.1	−25.60	−0.86			1	0.14	6.8	−25.01	0.47
		Sum	3.35	7.0	−23.42	1.67			Sum	6.02	5.1	−21.76	2.46
Site	A11	335	0.29	5.0	−21.85	4.15	Site	B5	335	0.48	4.8	−22.37	4.44
date	20/1/05	210	0.49	5.4	−23.36	3.81	date	31/1/05	210	1.37	4.5	−21.90	3.16
depth	60.9±0.8	55	0.73	6.6	−23.92	2.44	depth	58.9±1.6	55	1.47	5.2	−21.80	2.54
		20	0.73	6.8	−22.19	1.85			20	1.15	5.6	−21.26	2.60
		5	0.54	6.5	−22.48	0.68			5	0.28	6.0	−22.05	1.94
		1	0.16	7.6	−24.37	−0.40			1	0.14	8.1	−25.08	0.66
		Sum	2.94	6.2	−22.95	2.35			Sum	4.89	5.1	−21.86	2.89
Site	A11	335	0.17	5.3	−21.73	3.15	Site	B5	335	0.31	5.1	−23.47	3.75
date	20/1/05	210	0.31	5.4	−23.08	3.77	date	31/1/05	210	0.52	5.1	−23.14	2.79
depth	99.6±1.1	55	0.97	6.3	−22.53	2.36	depth	98.2±1.6	55	0.06	7.2	−25.32	2.32
		20	0.60	6.8	−21.78	1.29			20	0.17	6.3	−23.09	3.18
		5	0.45	7.0	−23.08	0.15			5	0.13	7.2	−23.61	3.09
		1	0.17	7.5	−24.06	0.19			1	0.14	8.1	−25.43	1.19
		Sum	2.67	6.4	−22.56	1.93			Sum	1.34	5.7	−23.60	2.97
Site	A11	335	0.07	5.8	−23.29	4.55	Site	B5	335	0.14	4.9	−23.68	4.29
date	20/1/05	210	0.17	5.6	−22.89	4.08	date	31/1/05	210	0.24	5.3	−23.72	4.08
depth	129.2±1.0	55	0.44	6.6	−22.32	2.36	depth	126.9±2.5	55	0.04	7.0	−25.35	1.91
		20	0.58	8.1	−20.14	−0.14			20	0.11	7.3	−23.36	2.35
		5	0.48	7.1	−21.88	−0.20			5	0.09	6.6	−23.64	2.56
		1	0.09	8.2	−23.21	0.81			1	0.08	8.7	−25.36	1.55
		Sum	1.84	7.1	−21.64	1.23			Sum	0.69	6.0	−23.93	3.42
Site	C11	335	0.04	5.7	−24.70	1.36	Site	A3	335	0.21	4.5	−21.27	3.44
date	26/1/05	210	0.35	4.9	−25.10	1.15	date	4/2/05	210	0.21	4.6	−21.09	3.12
depth	20.8±0.8	55	0.25	6.1	−23.95	0.73	depth	19.9±0.7	55	4.22	7.0	−20.52	1.00
		20	0.25	6.7	−22.45	0.56			20	0.01	9.0	iss	iss
		5	0.16	5.7	−24.98	−1.60			5	0.00	8.0	iss	iss
		1	0.08	6.3	−27.59	−3.22			1	0.12	7.0	−24.03	−0.14
		Sum	1.14	5.7	−24.39	0.30			Sum	4.77	6.7	−20.67	1.27
Site	C11	335	0.25	5.1	−24.86	1.18	Site	A3	335	0.28	4.2	−19.69	3.73
date	26/1/05	210	0.41	4.9	−25.87	1.20	date	4/2/05	210	0.34	4.3	−20.07	4.20
depth	60.1±0.7	55	0.31	6.0	−24.98	1.56	depth	58.6±0.8	55	4.04	6.8	−20.14	1.11
		20	0.25	6.1	−22.03	0.47			20	0.16	6.2	−23.71	4.08
		5	0.22	6.4	−24.36	0.42			5	0.00	6.3	iss	Iss
		1	0.10	7.3	−27.76	−3.18			1	0.16	6.4	−24.01	0.19
		Sum	1.53	5.6	−24.81	0.84			Sum	4.98	6.3	−20.35	1.71
Site	C11	335	0.20	5.0	−24.56	1.08	Site	A3	335	0.54	5.2	−19.83	4.77
date	26/1/05	210	0.67	5.5	−25.06	2.22	date	4/2/05	210	0.39	4.9	−20.79	4.99
depth	98.9±1.5	55	0.28	6.0	−24.69	1.13	depth	98.3±0.7	55	5.62	8.0	−19.56	1.60
		20	0.17	7.1	−23.42	−0.69			20	0.11	6.0	−21.75	3.85
		5	0.20	5.9	−23.21	−2.45			5	0.01	6.5	iss	iss
		1	0.07	7.7	−26.83	−2.61			1	0.09	7.0	−22.85	1.25
		Sum	1.58	5.7	−24.59	0.89			Sum	6.75	7.4	−19.74	2.29

Site	C11	335	0.20	5.1	−24.29	2.34	Site	A3	335	0.49	5.1	−21.07	5.05
date	26/1/05	210	0.20	6.0	−25.25	1.77	date	4/2/05	210	0.25	5.9	−20.96	6.13
depth	129.2±1.1	55	0.07	6.9	−26.82	1.26	depth	128.6±0.7	55	8.52	9.2	−18.77	1.62
		20	0.11	7.3	−23.98	−0.72			20	0.06	9.0	−24.33	Iss
		5	0.09	8.0	−24.65	−1.42			5	0.00	9.2	iss	Iss
		1	0.06	8.3	−27.38	−1.60			1	0.12	9.3	−22.57	1.61
		Sum	0.72	6.3	−25.03	1.10			Sum	9.45	8.7	−19.03	2.11
Site	B11	335	0.07	5.8	−25.30	0.73	Site	C5	335	0.35	4.3	−25.27	1.62
date	29/1/05	210	0.34	4.7	−24.88	0.22	date	7/2/05	210	0.27	4.3	−26.19	1.17
depth	19.3±0.5	55	0.20	5.3	−23.12	−0.58	depth	19.9±0.7	55	0.17	6.6	−25.39	0.89
		20	0.39	5.9	−20.98	−0.69			20	0.14	7.0	−21.98	1.42
		5	0.13	7.2	−23.69	−0.80			5	0.09	7.4	−24.11	0.32
		1	0.07	6.6	−26.65	−3.58			1	0.11	7.0	−27.91	−3.11
		Sum	1.21	5.5	−23.33	−0.44			Sum	1.13	5.2	−25.25	0.97
Site	B11	335	0.31	4.9	−24.13	0.43	Site	C5	335	0.23	5.3	−27.48	2.51
date	29/1/05	210	0.77	4.7	−25.71	0.60	date	7/2/05	210	0.30	4.8	−25.79	2.03
depth	58.4±0.8	55	0.24	5.5	−23.54	0.05	depth	59.1±0.9	55	0.35	5.3	−24.81	0.77
		20	0.39	5.9	−20.86	−0.71			20	0.25	5.8	−20.98	0.95
		5	0.18	5.7	−23.36	−1.69			5	0.13	6.2	−22.45	−0.74
		1	0.09	7.8	−26.75	−3.26			1	0.05	5.4	−27.23	−2.92
		Sum	1.98	5.2	−24.07	−0.02			Sum	1.30	5.4	−24.62	1.17
Site	B11	335	0.27	5.4	−24.02	−0.49	Site	C5	335	0.04	4.9	−24.30	1.75
date	29/1/05	210	0.63	5.8	−25.55	1.08	date	7/2/05	210	0.21	4.5	−25.66	2.38
depth	98.7±0.8	55	0.13	6.2	−24.74	−0.30	depth	99.8±1.8	55	0.18	5.3	−24.89	0.61
		20	0.21	7.4	−23.93	−0.49			20	0.13	6.4	−22.19	1.09
		5	0.12	6.5	−23.38	−1.08			5	0.09	5.9	−23.15	−0.36
		1	0.08	8.7	−26.81	−2.74			1	0.05	5.2	−26.74	−2.55
		Sum	1.44	6.1	−24.85	0.11			Sum	0.71	5.2	−24.48	1.01
Site	B11	335	0.11	5.2	−23.25	1.18	Site	C5	335	0.07	5.0	−24.98	3.39
date	29/1/05	210	0.28	5.9	−25.16	1.75	date	7/2/05	210	0.11	4.7	−25.41	2.76
depth	127±1.1	55	0.04	6.4	−26.17	1.77	depth	126.5±3.5	55	0.05	6.3	−25.54	1.64
		20	0.06	7.2	−24.71	−0.12			20	0.04	6.0	−24.14	0.93
		5	0.12	6.5	−24.17	−1.36			5	0.05	6.5	−23.98	0.23
		1	0.08	6.3	−26.98	−1.55			1	0.03	5.0	−26.67	−1.36
		Sum	0.69	6.0	−24.92	0.67			Sum	0.35	5.3	−25.12	1.91
Site	C1	335	0.29	6.4	−22.91	5.51							
date	9/2/05	210	0.37	4.6	−23.24	3.70							
depth	~20	55	0.17	5.6	−24.24	2.39							
		20	0.17	7.6	−23.32	2.43							
		5	0.21	8.1	−24.10	0.67							
		1	0.14	5.7	−26.24	−0.94							
		Sum	1.36	5.9	−23.75	2.91							

1. Sampling depth (dbar) precision is 1 sigma on the hose intake pressure. Depth for sample C1 estimated from hose length only.
2. Size-fractions were collected in series, with a 1000 μm pre-screen.
3. Sum indicates the values for the total of all size fractions and is not a separate measurement.

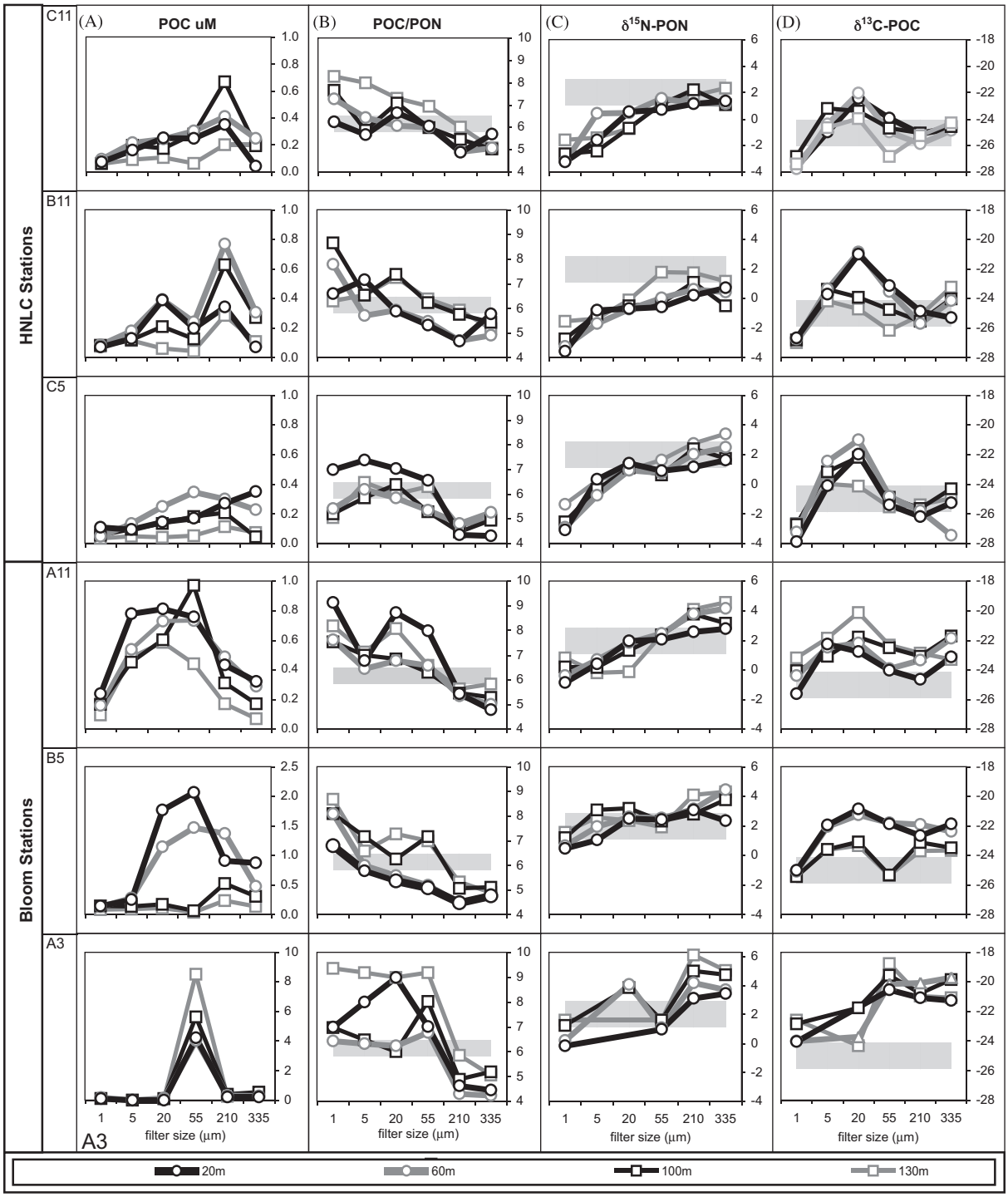

Fig. 4. Size-fractionated suspended-particle compositions: (A) POC (μM), (B) POC/PON, (C) δ^{15}N-PON (‰ vs. AIR), (D) δ^{13}C-POC (‰ vs. VPDB). Grey bands indicate (B) autotrophic POC/PON (5.7–6.6), (C) δ^{15}N-PON from nitrate assimilation (1–3‰), and (D) open Southern Ocean ^{13}C-POC (−26 to −24‰) for purposes of comparison (see text). Filter sizes are in μm.

bloom stations B5 and A3 (and the off-plateau moderate biomass station A11) show greater contributions from the diatom dominated 5, 20, and 55-μm fractions. In detail, the bloom stations vary from a narrow size distribution at A3, where the 55-μm fraction completely dominates the size distribution, to broader distributions across the 20, 55, and 210-μm fractions at B5 (and the 5, 20, 55, and 210-μm fractions at A11). These patterns hold for each depth sampled (20, 60, 100, and 130 m) except at station B5 where the two deepest samples do not show the enrichment in the diatom dominated middle size ranges.

The POC/PON ratios tend to decrease with increasing size fraction for almost all of the samples, from values of typically 7–9 in the smallest size fraction to 4–6 in the

largest fraction (Fig. 4B). The grey bands in Fig. 4B provide a reference for the range of expected values from autotrophic production (Redfield POC/PON = 6.6) to the somewhat lower POC/PON values (~5.7) observed for bulk suspended particles in many open Southern Ocean waters (Copin-Montegut and Copin-Montegut, 1983; Lourey and Trull, 2001). Most of the small fractions (1 and 5 μm) have values above this band, while the large fractions (210 and 335 μm) have values below this band, and the intermediate sizes (20 and 55 μm) have values close to the band. These patterns are suggestive of detrital (N-poor) contributions to the small fractions, zooplankton (N-rich) contributions to the large fractions, and autotrophic phytoplankton values for the intermediate sizes. However, on closer examination, this view breaks down. For example the diatom-dominated 55-μm fraction from surface waters at the A3 (and A11) bloom site lies well above the autotrophic band, while the same fraction from surface waters at the B5 bloom site lies well below it. This suggests that the POC/PON ratio reflects more than just the autotroph/heterotroph balance but also physiological status of the autotrophs. Samples taken from below the mixed layer have a tendency towards higher POC/PON ratios, consistent with preferential loss of organic nitrogen during remineralization, although this trend was also not observed at all sites.

3.5. δ^{15}N-PON of size-fractionated suspended particles: iron induced increases in *f*-ratios

Almost all the samples exhibit monotonic increases in δ^{15}N-PON with increasing particle size (Fig. 4C). The magnitude of this increase is typically ~4‰, but ranges from ~3‰ at B5 to ~5‰ at A3, which is equivalent to approximately 1–1.5 trophic levels based on the typical enrichment of 3–3.5‰ per trophic level (DeNiro and Epstein, 1981; Minagawa and Wada, 1984). Similar increases in δ^{15}N-PON with increasing size-fraction have been observed previously and have been attributed to trophic effects, with larger size classes containing proportionately more zooplankton grazers, including the supposition of a relatively low trophic enrichment for marine microbial trophic levels (Rau et al., 1990). However, the increase in δ^{15}N-PON with particle size probably reflects the combined effects of several processes. The higher values in the larger fractions (210 and 335 μm) probably reflect contributions from trophically ^{15}N-enriched zooplankton. The δ^{15}N-PON of the mid-size (20 and 55 μm) autotroph dominated fractions may represent the source value as set during photosynthesis from the nitrogen supply. The lower δ^{15}N-PON of the smaller fractions may represent the effects of greater uptake of recycled ammonium (which supplies ^{15}N-poor nitrogen) by small phytoplankton than large phytoplankton (e.g., Altabet, 1988, 1996; Karsh et al., 2003). The results for the shallow and deeper samples are very similar, suggesting that remineralization has not confounded the variations with size imprinted by production and trophic structure.

In principle, the contributions of ammonium recycling to the δ^{15}N-PON variations with size can be constrained by knowledge of the isotopic composition of new production. Combining the measured surface water δ^{15}N-NO_3 values with the closed system values for $^{15}\varepsilon_{NO_3}$ (Section 3.1) suggests that new production should produce PON with δ^{15}N of ~2–3‰ on the plateau and 1–2‰ off the plateau (i.e. new production has δ^{15}N-PON = δ^{15}N-NO_3-$^{15}\varepsilon_{NO_3}$). Accumulation of PON will lead to somewhat lower δ^{15}N-PON than that estimated in this way (for discussion and equations see Goericke et al., 1994; Sigman et al., 1999b; Karsh et al., 2003), but this effect will be much less than 1‰ given the small fractional extent of nitrate depletion (less than 30%) and PON accumulation (~1 μM and thus <15% of the nitrate depletion) during KEOPS. Thus a reasonable estimate for the δ^{15}N-PON of accumulated PON derived from nitrate is in the range of 1–3‰, as indicated by the grey bars in Fig. 4C.

This reference point for the δ^{15}N-PON from new production suggests that ammonium regeneration has significantly contributed to primary production in the small and mid-size fractions (1, 5, and 20 mm), since the δ^{15}N-PON values for those sizes lie below the range expected for new production (i.e. below the grey bars in Fig. 4C). In addition, these fractions have lower δ^{15}N-PON at the off-plateau HNLC sites than at the on-plateau bloom sites (Fig. 4C). This suggests that the increased iron supply over the plateau leads to greater new production, i.e. to higher *f*-ratios. We can estimate the relative use of ammonium and nitrate from a two end-member mixing model for the isotopic composition of the phytoplankton dominated size fractions:

$$\sum(\mathrm{PON}\,\delta^{15}\mathrm{N\text{-}PON})_i \Big/ \sum(\mathrm{PON})_i = f_{NO_3}\,\delta^{15}\mathrm{N\text{-}PON}_{NO_3} + (1-f_{NO_3})\delta^{15}\mathrm{N\text{-}PON}_{NH_4}$$

and thus obtain estimates of the fraction of production based on nitrate, f_{NO_3}, i.e. *f*-ratios. Taking the sum Σ_i over the small and intermediate size-fractions (1, 5, 20, and 55 μm) and assuming that phytoplankton that assimilate only nitrate have δ^{15}N-PON_{NO_3} of +3‰ (i.e. δ^{15}N-PON_{NO_3} equivalent to the top of the grey reference bars in Fig. 4C) and phytoplankton that assimilate only ammonium have δ^{15}N-PON_{NH_4} of −3‰ (i.e. the lowest value observed in any fraction) we estimate an increase in *f*-ratios from 0.4–0.6 off-plateau to 0.7–0.9 on-plateau (Table 4, Model 1).

These *f*-ratio estimates are of course dependent on the end-member values. If we use δ^{15}N-PON_{NH_4} of −6‰ to accommodate (i) the probability that we have not observed the pure ammonium-based end-member in our size fractions, and (ii) the fact that lower ratios of δ^{15}N-PON have been observed in other Southern Ocean surface waters (Lourey et al., 2003), we obtain higher *f*-ratios at all sites, as well as a smaller increase from off-plateau 0.6–0.7 to

Table 4
F-ratio estimates from size-fractionated δ^{15}N-PON compositions

	Depth (m)	Model 1 *f*-ratios $\delta^{15}N\text{-}PON_{NO_3} = +3$ $\delta^{15}N\text{-}PON_{NH_4} = -3$	Model 2 *f*-ratios $\delta^{15}N\text{-}PON_{NO_3} = +3$ $\delta^{15}N\text{-}PON_{NH_4} = -6$	Model 3 *f*-ratios $\delta^{15}N\text{-}PON_{NO_3} = +5$ $\delta^{15}N\text{-}PON_{NH_4} = -3$
Bloom sites				
A3	20	0.66	0.77	0.50
	60	0.70	0.80	0.52
B5	20	0.89	0.93	0.67
	60	0.91	0.94	0.68
A11	20	0.70	0.80	0.53
	60	0.77	0.85	0.58
HNLC sites				
C11	20	0.45	0.64	0.34
	60	0.58	0.72	0.44
B11	20	0.35	0.57	0.26
	60	0.35	0.57	0.27
C5	20	0.52	0.68	0.39
	60	0.56	0.71	0.42

Calculated for the summed fractions dominated by phytoplankton (1, 5, 20, and 55 μm).

0.8–0.9 on-plateau (Table 4, Model 2). Alternatively, assuming a higher $\delta^{15}N\text{-}PON_{NO_3}$ of 5‰, based on laboratory experiments that exhibit low $^{15}\varepsilon_{NO_3}$ of 1–2‰ (Waser et al., 1999; Needoba et al., 2003), we obtain *f*-ratios of 0.3–0.4 off-plateau and 0.5–0.7 on-plateau (Table 4, Model 3). This last choice necessarily implies that the present isotopic fractionation accompanying PON production differs from the seasonal average as constrained by the nitrate isotopic compositions. Overall, we prefer model 1 because its end-member values are most closely in accord with all our observations and require the simplest set of assumptions.

While the best choice of end-members in the model is debatable, all choices clearly identify a strong increase in nitrate-based production over the plateau. This is in accord with *f*-ratio estimates for surface waters (<20 m depth) from shipboard incubations with ^{15}N-enriched ammonium and nitrate (Mosseri et al., 2008; Raimbault et al., in preparation), that suggest *f*-ratios of ~0.3 off-plateau (C11) and ~0.6 on-plateau (A3). The tracer incubations provide greater temporal resolution and suggest that values on-plateau at A3 had declined to levels similar to off-plateau values by the end of the shipboard observation period. Temporal variations could also explain the lower *f*-ratios obtained at A3 than at B5 from our data, if senescing blooms proceed from nitrate towards ammonium use over time. The bloom at B5 developed during the KEOPS shipboard period (from about January 25, 2005 onward; Mongin et al., 2008; Mosseri et al., 2008) presumably in response to increased iron supply, whereas the A3 bloom was in decline. Our approach provides a measure of the average *f*-ratio over the residence time of PON in surface waters and thus complements the short-term incubations, while avoiding the potential for incubation artefacts.

3.6. δ^{13}C-POC of size-fractionated suspended particles: iron induced increases in phytoplankton growth rates

The structure of the size-fractionated δ^{13}C-POC compositions also varies between the off-plateau and on-plateau sites (Fig. 4D). The grey bands in Fig. 4D provide a reference for values found in open Southern Ocean HNLC waters in the Polar Frontal Zone and ice-free Antarctic Zone south of Australia (Trull and Armand, 2001; Lourey et al., 2004). The off-plateau HNLC sites C11 and B11 have maximal values in the 20–55-μm size fraction. This structure is also seen strongly at the plateau-periphery site C5 and weakly at the A11 off-plateau site. At the on-plateau bloom sites this structure is weaker at B5 and disappears at A3 because the larger size fractions (55, 210, and 335 μm) also have high δ^{13}C-POC.

As with the bulk samples (Fig. 3D), the individual size fractions (especially the 20-μm fraction) show both decreases (stations C11, B11, C5, B5) and increases (stations A3 and A11) in δ^{13}C-POC with depth (Fig. 4D). The decreases with depth could result from remineralization, as some studies have suggested that lipids, which have low δ^{13}C values, are not remineralized as fast as more ^{13}C-rich proteins and carbohydrates (e.g., as reviewed by Altabet, 1996), but we do not have sufficient data to confirm this. A speculative explanation for the opposite patterns at A3 and A11, motivated by the presence of subsurface maxima in chlorophyll at these sites (Mosseri et al., 2008) and total POC concentrations at A3 (Fig. 3A), is that this represents biomass produced at higher growth rates at an earlier time that has subsequently settled.

The off-plateau δ^{13}C-POC maximum in mid-size fractions has been observed before in HNLC waters during the SOIREE iron fertilization experiment (Trull and Armand, 2001). At that time the increase in δ^{13}C-POC with size in

the smaller fractions (1, 5, 20, and 55 μm) was attributed to variable fractionation during autotrophic assimilation following the supply vs. demand model for diffusive CO_2 limitation of isotopic fractionation (Laws et al., 1995; Popp et al., 1998, 1999). That is, the higher δ^{13}C-POC of larger phytoplankton derives from greater consumption of their internal pool of carbon dioxide, because diffusive exchange with seawater does not as readily keep up with consumption in large cells as it does in small cells. The decrease in δ^{13}C-POC in the largest size fractions (210, 355 μm) was attributed to the presence of small copepods, which were feeding on and thus had similar compositions to the smallest phytoplankton size classes (1, 5-μm fractions). Extending these analyses to the KEOPS sites would imply that the zooplankton in the larger size classes (210, 335 μm) were feeding on the smaller phytoplankton size classes (5, 20 μm) off-plateau, but on the larger phytoplankton size classes (55 μm) that were more plentiful on-plateau. This interpretation would be consistent with the tendency of the zooplankton populations to include large copepods on-plateau (Carlotti et al., 2008).

The variations of δ^{13}C-POC across the size-classes (Fig. 4D) suggest that the higher total δ^{13}C-POC observed on-plateau than off-plateau (Fig. 3D) is driven by the presence of more large phytoplankton on-plateau and probably also by higher growth rates. In order to quantify these changes, we must first account for the greater depletion of DIC over the plateau and its associated ^{13}C enrichment. δ^{13}C-DIC compositions were not measured, but can be estimated from phosphate depletion (Lynch-Stieglitz et al., 1995):

$$\delta^{13}C_{DIC} = \delta^{13}C^{o}_{DIC} + \Delta_{bio}\left[\frac{(PO_4 - PO_4^o)(C:P)_{bio}}{DIC^o}\right]$$

The initial conditions can be estimated from observed temperature-minimum estimates of Winter Water values for DIC^o (2178 μM) and PO_4^o (2.4 μM) from Jouandet et al. (2008) and Blain et al. (2007). A reasonable estimate for $\delta^{13}C^o_{DIC}$ is that of the Circumpolar Deep Water Source of nutrients to the Southern Ocean, which is close to 0.3‰ at 2.4 μM PO_4^{3-} (Lynch-Stieglitz et al., 1995). For the observed summer PO_4 concentrations at C11 (2.2 μM) and A3 (1.25 μM), Redfield-ratio nutrient consumption, i.e. $(C:P)_{bio}$ of 128, and associated isotopic fractionation of −25‰ for Δ_{bio} (δ^{13}C-POC-$\delta^{13}C_{DIC}$), the expected values for $\delta^{13}C_{DIC}$ are 0.9‰ at C11 and 2‰ at A3.

These estimates are of course approximations, because they do not include the effects of air–sea CO_2 exchange or seasonal alkalinity export, but are nonetheless close to values observed in the Southern Ocean Polar Frontal and Antarctic Zones (Lynch-Stieglitz et al., 1995; Trull and Armand, 2001) and near Kerguelen Island, where δ^{13}C-DIC values of 1.7–1.8‰ were observed in chlorophyll-rich waters over the shelf in early autumn (Bentaleb et al., 1998). Because we have used a Δ_{bio} estimate at the top of the range suggested from the total δ^{13}C-POC (Fig. 3D) and size-fractionated δ^{13}C-POC (Fig. 4D) observations, and because alkalinity export is generally small in the Polar Frontal and Antarctic Zone (Trull and Armand, 2001; Trull et al., 2001a; Lourey et al., 2004), these estimates are likely to be maxima, as is the difference between them of 1.1‰ for the DIC depletion-driven differences in on-plateau and off-plateau δ^{13}C-POC compositions. This view is confirmed by comparison to observations along a transect from Kerguelen Island high biomass shelf waters north into moderate biomass waters, which revealed a decrease in δ^{13}C-DIC from approximately 1.8–1.2‰ (Bentaleb et al., 1998). Thus the ^{13}C enrichment associated with DIC draw-down is expected to represent only a small portion of the overall range in δ^{13}C-POC of more than 5‰ observed during KEOPS (Fig. 3D).

The seasonal depletion of DIC also may lead to higher ^{13}C contents of phytoplankton by another mechanism—the associated reduction of molecular CO_2 concentrations. Laboratory and field studies have shown that phytoplankton grown in the presence of low molecular CO_2 tend to be ^{13}C-rich (Laws et al., 1995; Bentaleb et al., 1998; Popp et al., 1998), although debate continues about whether this reflects greater consumption of the internal cellular CO_2 pool, or increased utilization of HCO_3^- (Tortell et al., 2000; Cassar et al., 2002, 2004). The observed surface temperatures and pCO_2 values (Blain et al., 2007; Jouandet et al., 2008) at C11 (370 μatm) and A3 (315 μatm) yield molecular CO_2 concentrations of 21.7 and 17.5 μM, respectively. This is a relatively large difference in terms of its affects on δ^{13}C-POC. For example, the correlation of δ^{13}C-POC with the reciprocal of molecular CO_2 concentrations observed in Sub-Antarctic and Polar Frontal Zone waters south of Australia (Lourey et al., 2004) suggests that the decreased molecular CO_2 concentration over the plateau would be sufficient to increase δ^{13}C-POC by 1.8‰. The magnitude of this effect is very similar to predictions based on linear and reciprocal correlations developed for waters near and north of Kerguelen Island, which suggest an increase in δ^{13}C-POC of 1.9‰ and 2.3‰, respectively, (as calculated from Eqs. (2) and (3) of Bentaleb et al., 1998). The model of Rau et al. (1997), fit to a global compilation of surface δ^{13}C-POC, suggests a similar increase of 2–2.5‰ over the plateau (for cells of 10 μm equivalent spherical diameter and increasing with growth rate from 0.5 to 1.0 d^{-1}). The model of Popp et al. (1998), based on laboratory results adjusted for cell surface to volume ratios and varying growth rates, suggests that we might expect to observe an increase of 1.7–3.4‰ in δ^{13}C-POC (again for cells of 10 μm equivalent spherical diameter and increasing with growth rate from 0.5 to 1.0 d^{-1}). Thus, based on the Southern Ocean field results, the lower molecular CO_2 concentrations over the plateau may account for ~2‰ of the ~5‰ increase in ^{13}C-POC over the plateau, while the laboratory experiments for rapidly growing cells suggest it may account for somewhat more, ~3‰ of the 5‰. Thus other factors must contribute, including phytoplankton size and growth rate, as has also been found during the SOIREE iron fertilization experiment (Trull and Armand, 2001) and

in the highly productive waters near Kerguelen Island (Bentaleb et al., 1998).

The 55–210-μm size-fraction exhibits the greatest elevation of δ^{13}C-POC over the plateau (Fig. 4D). In particular, at station A3 where this size-fraction dominates biomass, δ^{13}C-POC is ~−20‰, and thus 3–5‰ higher than values in this size-fraction at the off-plateau stations. Correcting for the effects of ^{13}C-DIC enrichment and molecular CO_2 depletion leaves 0–2‰ that may be attributable to increased growth rates. Based on the models of Rau et al. (1997) and Popp et al. (1998), a 25% increase in growth rate would be sufficient to produce 2‰ enrichment in δ^{13}C-POC. This inference is in keeping with only moderately higher growth rates over the plateau (~0–40%) estimated from the ~8-fold higher ^{13}C and ^{14}C primary production rates over the plateau (Lefèvre et al., 2008) when scaled to ~5–8-fold higher chlorophyll inventories (Mosseri et al., 2008).

When fully dissected, it appears that the much higher δ^{13}C-POC over the plateau may derive from the sum of all the effects of the bloom, rather than enhanced phytoplankton production alone. These include the effects of nutrient depletion (via both ^{13}C-DIC enrichment and molecular CO_2 depletion) and higher phytoplankton growth rates (via direct affects on phytoplankton isotopic fractionation), but also the ecosystem scale implications of higher growth rates, including the escape of large ^{13}C-rich phytoplankton from grazing pressure and the ensuing development of a ^{13}C-enriched phytoplankton community.

3.7. Sinking particles from the free-drifting sediment traps: controls on export

One of the anticipated outcomes of KEOPS was a better quantification of export processes than has been achieved during artificial iron fertilization experiments. Failure to recover most of the drifting sediment traps has frustrated this goal to some degree and increased the reliance on indirect measures. The ^{234}Th deficit method suggests that POC export over the plateau was approximately double that of surrounding HNLC waters (Blain et al., 2007; Savoye et al., 2008). The increase in primary production over the plateau was larger than this, ~3–4 times higher than off the plateau (as estimated from ^{13}C and ^{14}C uptake experiments, (Mosseri et al., 2008). The elevation of net community production was even larger, up to 10-fold higher over the plateau, although this enhancement did not persist to the end of the field programme (as estimated from O_2 and DIC changes in bottle incubations; Lefèvre et al., 2008). The smaller increase in export than in primary production and net-community production may partly reflect greater biomass accumulation but also stronger recycling over the plateau, which is consistent with greater bacterial activity over the plateau (Obernosterer et al., 2008). Examination of particulate barium distributions also shows differences on and off the plateau, and has been suggested to indicate smaller fractional export of the standing stock of particles on-plateau than off-plateau, but subsequently greater remineralization of these particles off-plateau at mesopelagic depths (Jacquet et al., 2008).

We can only compare trap samples from the central bloom site (A3i and A3f deployments) with those at the plateau periphery site (C5 deployment). The flux of POC was highest during the A3i deployment, and lower during A3f and at C5 (Table 5). The 2–3-fold higher flux at A3i than at C5 is consistent with results based on ^{234}Th, which suggest a 4-fold difference between these sites (Savoye et al., 2008). However, the absolute fluxes measured by the traps were considerably lower than expected from the ^{234}Th results (3-fold for A3i; 8-fold for C5). This difference could represent real short-term variations in the sinking flux during the demise of the bloom as seen in satellite images (Blain et al., 2007; Mongin et al., 2008) since the trap collected for ~1 day (Table 5) and the establishment of the ^{234}Th disequilibria represents export over several weeks.

Table 5
Drifting sediment trap particle fluxes and compositions

Site[a]	Date	Cup no.	Cup duration (h)	Size-fraction (μm)	POC flux (μmol m^{-2} h^{-1})	POC/PON (mol/mol)	δ^{13}C-POC ‰ PDB	δ^{15}N-PON ‰ AIR
A3i	4 Feb. 05	1	2	>350	289	6.0	−21.20	7.63
		2	2	1-350	141	7.3	−21.58	2.27
		3	6	>350	140	5.6	−22.81	5.91
		4	6	1-350	166	7.4	−20.97	3.27
C5	7 Feb. 05	5	4	>350	423	4.7	−25.10	5.10
		6	4	1-350	63	6.9	−23.57	0.01
		7	6	>350	200	4.5	−25.09	4.58
		8	6	1-350	68	6.6	−23.24	0.43
A3f	12 Feb. 05	9	3	>350	80	5.1	−21.54	5.67
		10	3	1-350	45	9.4	−22.54	2.57
		11	8	>350	63	5.1	−20.97	6.06
		12	8	1-350	68	6.3	−23.74	4.01

[a]All samples collected at 200 m depth using the Technicap PPS3/3 trap—see Section 2 for details.

Alternatively, it may reflect non-ideal collection, since traps are known to experience 2–3-fold flux variations in response to hydrodynamic effects (Gardner, 2000; Buesseler et al., 2006). The need for caution in interpreting the flux variations is reinforced by the large fraction of the total trap material, which was discounted as having entered the trap as "swimmers" (50–65% at A3i and up to 90% at C5). In this light, the variability of the individual cup POC fluxes for each deployment is surprisingly small (less than a factor of two; Table 5), although good precision is of course not an indication of accuracy.

Differences in the controls on export between the A3 and C5 sites is suggested by comparing the trap results with the total suspended particle compositions. At A3, the sinking materials were enriched in δ^{15}N-PON in comparison to suspended compositions in the mixed layer (Fig. 3C). This is similar to observations from many open-ocean locations, and has been generally interpreted as preferential export of large nitrate assimilating ^{15}N-rich phytoplankton in comparison to ammonium-regeneration derived ^{15}N-poor small phytoplankton (Altabet, 1988, 1989, 1996). Comparison of δ^{15}N-PON in exported material to the size-fractionated suspended δ^{15}N-PON shows that at the bloom site A3, the export of larger autotrophs (20, 55 μm fractions) would be consistent with the export of PON with δ^{15}N that is higher than the bulk suspended PON. Alternatively, given that faecal pellets tend to be enriched by ~2.2‰ with respect to the food source (Altabet and Small, 1990), the export of faecal pellets from zooplankton that feed on the bulk autotroph community would also offer a good match with the trap compositions (Figs. 3C and 4C). Examination of the forms of the sinking particles as revealed by particles collected in polyacrylamide gels (Ebersbach and Trull, 2008) favours control by zooplankton faecal pellet flux and associated ^{15}N enrichment.

In contrast, at the C5 bloom periphery trap site, the sinking particles have lower δ^{15}N-PON (0.0–0.4‰) than the mixed-layer total suspended δ^{15}N-PON (1.0–1.2‰), suggesting a preferential contribution from smaller (1 and 5 μm) size fractions, which have lower values (0.3 to as low as −3.1; Table 3). Export of small phytoplankton within large aggregates has been documented in Sub-Antarctic waters east of New Zealand (Waite et al., 2000) and pico-phytoplankton did dominate C5 surface waters in contrast to all other stations (Griffiths and Uitz, 2006). However, the δ^{13}C-POC compositions also show differences between the A3 and C5 sites that contrast with the δ^{15}N-PON patterns between the sinking and suspended particle compositions. For δ^{13}C-POC, lower values were observed in the sinking flux at A3 and higher values in the sinking flux at C5 (Fig. 3D). This is the opposite of what would be expected if large ^{13}C-rich phytoplankton dominated export at A3 and small ^{13}C-poor phytoplankton influenced export at C5. Thus, control by zooplankton grazing that fractionated compound classes (e.g., consuming varying amounts of ^{13}C-poor lipids) appears more likely. In addition, bacterial remineralization can decrease marine δ^{13}C-POC values by ~1‰ via selective degradation of some compound classes (Altabet, 1996; Freeman, 2001).

4. Conclusions

Our observations are consistent with an influence of natural iron fertilization on nitrogen and carbon metabolism in the Southern Ocean in late summer. The phytoplankton isotopic compositions indicate faster growth rates, and a shift from ammonium towards assimilation of nitrate as a nitrogen source. The size structure of the microbial community becomes biased towards greater numbers of larger phytoplankton, and an increase in the ratio of autotrophs to heterotrophs (at least for the <1000 μm ecosystem components studied here). This restructuring of the food-web leads to greater export fluxes, although the efficiency of export as a fraction of primary production appears to have somewhat decreased (Savoye et al., 2008). Similar conclusions have also been reached from incubation-based metabolic rate measurements (Lefèvre et al., 2008; Mosseri et al., 2008), and microscopic examination of microbial and zooplankton community structure (Armand et al., 2008; Obernosterer et al., 2008; Carlotti et al., 2008). Our approach complements those efforts. In contrast to the microscopic studies, it offers the advantage of direct quantification of the nutrient elements (C and N) assimilated by the microbial ecosystem. It also avoids the possibility of incubation artefacts. However, the stable isotope approach requires detailed knowledge of isotopic fractionation processes and factors and will become more precise as this knowledge increases.

Acknowledgements

We thank Stéphane Blain, Bernard Quéguiner, and Catherine Jeandel for inviting and supporting our participation in KEOPS. The Institute Polaire Emil Victoire, the captain and crew of the Marion Dufresne, the Australian Commonwealth Cooperative Research Centre Program, CSIRO Marine and Atmospheric Research, the French-Australian Science and Technology Cooperation (Award #FR040170), and the Australian Antarctic Science Program (AAS#1156) provided logistic and financial support. Sediment trap equipment was loaned from the US NSF VERTIGO project (K. Buesseler, T. Trull et al. Award #0301139). The University of Tasmania, the Australian Academy of Sciences, and the Observatoire Midi-Pyrenees provided financial support during the synthesis of these results while Tom Trull was on study leave at the Woods Hole Oceanographic Institution, MA, USA and the Laboratoire d'Etudes Geophysiques et Oceanographiques Spatiales, Toulouse, France. Steve Bray (ACE) and Lisette Robertson (ACE) prepared the pump and filtration equipment. Steve Bray, Danny Mclaughlin (CMAR), Jim Valdes and John Andrews (WHOI), and Nathalie Leblond (INSU) prepared the surface-tethered trap equipment.

Friederike Ebersbach (ACE) assisted with onboard filtering. Matt McIlvin (WHOI) did the nitrate isotopic analyses. Nicole Garcia (U. Marseille) did the shipboard nutrient analyses and Val Latham (CMAR) the laboratory nitrate analyses. Graham Rowbottom did the POC and PON analyses in the University of Tasmania Central Sciences Laboratory. Nicole Garcia and Patrick Raimbault (U. Marseille) shared their ^{15}N tracer uptake results, and Peter DiFiore and Danny Sigman (Princeton U.) shared their nitrate isotope results prior to publication. Constructive comments from Ihlem Bentaleb, Peter Thompson, John Volkman, Francois Lacan and an anonymous reviewer greatly improved this paper.

References

Abraham, E.R., Law, C.S., Boyd, P.W., Lavender, S.J., Maldonado, M.T., Bowie, A.R., 2000. Importance of stirring in the development of an iron-fertilized phytoplankton bloom. Nature 407, 727–730.

Altabet, M.A., 1988. Variations in nitrogen isotopic composition between sinking and suspended particles: implications for nitrogen cycling and particle transformation in the open ocean. Deep-Sea Research 35 (4), 535–554.

Altabet, M.A., 1989. A time-series study of the vertical structure of nitrogen and particle dynamics in the Sargasso Sea. Limnology and Oceanography 34 (7), 1185–1201.

Altabet, M.A., 1996. Nitrogen and carbon isotopic tracers of the source and transformation of particles in the deep sea. In: Ittekkot, V., Schafer, P., Honjo, S., Depetris, P.J. (Eds.), Particle Flux in the Ocean. Wiley, New York, pp. 155–184.

Altabet, M.A., Francois, R., 1994. Sedimentary nitrogen isotopic ratio as a recorder for surface ocean nitrate utilization. Global Biogeochemical Cycles 8 (1), 103–116.

Altabet, M.A., Francois, R., 2001. Nitrogen isotope biogeochemistry of the Antarctic Polar Frontal Zone at 170°W. Deep-Sea Research II 48, 4247–4273.

Altabet, M.A., Small, L.F., 1990. Nitrogen isotopic ratios in fecal pellets produced by marine zooplankton. Geochimica Cosmochimica Acta 54 (7), 155–163.

Altabet, M.A., Deuser, W.G., Honjo, S., Stienen, C., 1991. Seasonal and depth-related changes in the source of sinking particles in the North Atlantic. Nature 354, 136–139.

Armand, L.K., Cornet-Barthaux, V., Mosseri, J., Quéguiner, B., 2008. Late summer diatom biomass and community structure on and around the naturally iron-fertilized Kerguelen Plateau in the Southern Ocean. Deep-Sea Research II, this issue [doi:10.1016/j.dsr2.2007.12.031].

Bentaleb, I., Fontugne, M., Descolas-Gros, C., Girardin, C., Mariotti, A., Pierre, C., Brunet, C., Poisson, A., 1998. Carbon isotopic fractionation by plankton in the Southern Indian Ocean: relationship between $\delta^{13}C$ of particulate organic carbon and dissolved carbon dioxide. Journal of Marine Systems 17, 39–58.

Bianchi, M., Feliatra, F., Treguer, P., Vincendeau, M.-A., Morvan, J., 1997. Nitrification rates, ammonium and nitrate distribution in upper layers of the water column and in sediments of the Indian sector of the Southern Ocean. Deep-Sea Research I 44 (5), 1017–1032.

Blain, S., Quéguiner, B., Armand, L., Belviso, S., Bombled, B., Bopp, L., Bowie, A., Brunet, C., Brussaard, C., Carlotti, F., Christaki, U., Corbière, A., Durand, I., Ebersbach, F., Fuda, J.L., Garcia, N., Gerringa, L., Griffiths, B., Guigue, C., Guillerm, C., Jacquet, S., Jeandel, C., Laan, P., Lefèvre, D., Lomonaco, C., Malits, A., Mosseri, J., Obernosterer, I., Park, Y.-H., Picheral, M., Pondaven, P., Remenyi, T., Sandroni, V., Sarthou, G., Savoye, N., Scouarnec, L., Souhaut, M., Thuiller, D., Timmermans, K., Trull, T., Uitz, J., van-Beek, P., Veldhuis, M., Vincent, D., Viollier, E., Vong, L., Wagener, T., 2007. Impacts of natural iron fertilisation on the Southern Ocean. Nature 446, 1070–1074.

Blain, S., Sarthou, G., Laan, P., 2008. Distribution of dissolved iron during the natural iron-fertilization experiment KEOPS (Kerguelen Plateau, Southern Ocean). Deep-Sea Research II, this issue [doi:10.1016/j.dsr2.2007.12.028].

Bohlke, J.K., Mroczkowski, S.J., Coplen, T.B., 2003. Oxygen isotopes in nitrate: new reference materials for ^{18}O:^{17}O:^{16}O measurements and observations on nitrate-water equilibration. Rapid Communications in Mass Spectrometry 17, 1835–1846.

Boyd, P.W., Newton, P., 1995. Evidence of the potential influence of planktonic community structure on the interannual variability of particulate carbon flux. Deep-Sea Research I 42, 619–639.

Boyd, P.W., Newton, P., 1999. Does planktonic community structure determine downward particulate organic carbon flux in different oceanic provinces? Deep-Sea Research I 46, 63–91.

Boyd, P., Watson, A., Law, C.S., Abraham, E., Trull, T., Murdoch, R., Bakker, D.C.E., Bowie, A., Buesseler, K.O., Chang, H., Charette, M., Croot, P., Downing, K., Frew, R., Gall, M., Hadfield, M., Hall, J., Harvey, M., Jameson, G., La Roche, J., Liddicoat, M., Ling, R., Maldonado, M., McKay, R.M., Nodder, S., Pickmere, S., Pridmore, R., Rintoul, S., Safi, K., Sutton, P., Strzepek, R., Tanneberger, K., Turner, S., Waite, A., Zeldis, J., 2000. A mesoscale phytoplankton bloom in the polar Southern Ocean stimulated by iron fertilization. Nature 407, 695–702.

Boyd, P.W., Jackson, G.A., Waite, A.M., 2002. Are mesoscale perturbation experiments in polar waters prone to physical artefacts? Evidence from algal aggregation modelling studies. Geophysical Research Letters 29 (11).

Brooks, P.D., Geilmann, H., Werner, R.A., Brand, W.A., 2003. Improved precision of coupled ^{13}C and ^{15}N measurements from single samples using an elemental analyser. Rapid Communications in Mass Spectroscopy 17, 1924–1926.

Buesseler, K.O., Andrews, J.E., Pike, S.M., Charette, M.A., Goldson, L.E., Brzezinski, M.A., Lance, V.P., 2005. Particle export during the Southern Ocean Iron Experiment (SOFeX). Limnology and Oceanography 50 (1), 311–327.

Buesseler, K.O., Antia, A.N., Chen, M., Fowler, S.W., Gardner, W.D., Gustafsson, O., Harada, K., Michaels, A.F., Rutgers van der Loeff, M., Sarin, M., Steinberg, D.K., Trull, T., 2006. Estimating upper ocean particle fluxes with sediment traps: a progress report. Journal of Marine Research 65 (3), 345–416.

Carlotti, F., Thibault-Botha, D., Nowaczyk, A., Lefèvre, D., 2008. Zooplankton community structure, biomass and role in carbon fluxes during the second half of a phytoplankton bloom in the eastern sector of the Kerguelen Shelf (January–February 2005). Deep-Sea Research II, this issue [doi:10.1016/j.dsr2.2007.12.010].

Casciotti, K., Sigman, D.M., Galanter Hastings, M., Bohlke, J.K., Hilkert, A., 2002. Meaurement of the oxygen isotopic composition of nitrate in seawater and freshwater using the denitrifier method. Analytical Chemistry 74, 4905–4912.

Cassar, N., Laws, E.A., Popp, B.N., Bidigare, R.R., 2002. Sources of carbon for photosynthesis in a strain of Phaeodactylum tricornutum. Limnology and Oceanography 47 (4), 1192–1197.

Cassar, N., Laws, E.A., Bidigare, R.R., Popp, B.N., 2004. Bicarbonate uptake by Southern Ocean phytoplankton. Global Biogeochemical Cycles 18.

Coale, K.H., Johnson, K.S., Chavez, F.P., Buesseler, K.O., Barber, R.T., Brzezinski, M.A., Cochlan, W.P., Millero, F.J., Falkowski, P.G., Bauer, J.E., Wanninkhof, R.H., Kudela, R.M., Altabet, M.A., Hales, B.E., Takahashi, T., Landry, M.R., Bidigare, R.R., Wang, X., Chase, Z., Strutton, P.G., Friederich, G.E., Gorbunov, M.Y., Lance, V.P., Hilting, A.K., Hiscock, M.R., Demarest, M., Hiscock, W.T., Sullivan, K.F., Tanner, S.J., Gordon, R.M., Hunter, C.N., Elrod, V.A., Fitzwater, S.E., Jones, J.L., Tozzi, S., Koblizek, M., Roberts, A.E., Herndon, J., Brewster, J., Ladizinsky, N., Smith, G., Cooper, D., Timothy, D., Brown, S.L., Selph, K.E., Sheridan, C.C., Twining, B.S., Johnson, Z.I., 2004. Southern Ocean iron enrichment experiment: carbon cycling in high and low-Si waters. Science 304, 408–414.

Copin-Montegut, C., Copin-Montegut, G., 1983. Stoichiometry of carbon, nitrogen, and phosphorus in marine particulate matter. Deep-Sea Research 30 (1), 31–46.

DeNiro, M.J., Epstein, S., 1981. Influence of diet on the distribution of nitrogen isotopes in animals. Geochimica Cosmochimica Acta 45, 341–351.

DiFiore, P., Sigman, D.M., Trull, T.W., Lourey, M.J., Karsh, K., Cane, G., Ho, R., 2006. Nitrogen isotope constraints on Subantarctic biogeochemistry. Journal of Geophysical Research 111, C08016.

Ebersbach, F., Trull, T.W., 2008. Sinking particle properties from polyacrylamide gels during KEOPS: zooplankton control of carbon export in an area of persistent natural iron inputs in the Southern Ocean. Limnology and Oceanography 53, 212–224.

Francois, R., Altabet, M.A., Burckle, L.H., 1992. Glacial to interglacial changes in surface nitrate utilization in the Indian sector of the Southern Ocean as recorded by sediment $\delta^{15}N$. Paleoceanography 7 (5), 589–606.

Francois, R., Altabet, M.A., Yu, E.-F., Sigman, D.M., Bacon, M.P., Frank, M., Bohrmann, G., Bareille, G., Labeyrie, L.D., 1997. Contribution of Southern Ocean surface-water stratification to low atmospheric CO_2 concentration during the last glacial period. Nature 389, 929–935.

Freeman, K.H., 2001. Isotope biogeochemistry of marine organic carbon. In: Valley, J.W., Cole, D.R. (Eds.), Stable Isotope Geochemistry. Reviews in Mineralogy and Geochemistry. Mineralogical Society of America, Washington, DC, pp. 579–606.

Fry, B., Sherr, E.B., 1984. $\delta^{13}C$ measurements as indicators of carbon flow in marine and freshwater ecosystems. In: Rundel, P.W., Ehleringer, J.R., Nagy, K.A. (Eds.), Stable Isotopes in Ecological Research. Springer, New York, pp. 196–229.

Gardner, W.D., 2000. Sediment trap sampling in surface waters. In: Hanson, R.B., Ducklow, H.W., Field, J.G. (Eds.), The Changing Ocean Carbon Cycle: a midterm synthesis of the Joint Global Ocean Flux Study. International Geosphere–Biosphere Programme Book Series. Cambridge University Press, Cambridge, pp. 240–281.

Geider, R.J., La Roche, J., 2004. The role of iron in phytoplankton photosynthesis, and the potential for iron-limitation of primary productivity in the sea. Photosynthesis Research 39 (3), 275–301.

Goericke, R., Montoya, J.P., Fry, B., 1994. Physiology of isotopic fractionation in algae and cyanobacteria. In: Lajtha, K., Michener, R.H. (Eds.), Stable Isotopes in Ecology and Environmental Science. Blackwell Scientific Publications, Oxford, pp. 1221–1870.

Granger, J., Sigman, D.M., Needoba, J., Harrison, P.J., 2004. Coupled nitrogen and oxygen isotope fractionation of nitrate during assimilation by cultures of marine phytoplankton. Limnology and Oceanography 49 (5), 1763–1773.

Griffiths, F.B., Uitz, J., 2006. Photosynthetic Parameters, Size-Fractionated Chlorophyll and Primary Production During the KEOPS Expedition East of Kerguelen Island January–February 2005. ASLO-TOS-AGU Ocean Sciences Meeting Abstract, OS35M-09.

Hayes, J.M., 2001. Fractionation of carbon and hydrogen isotopes in biosynthetic processes. In: Valley, J.W., Cole, D.R. (Eds.), Stable Isotope Geochemistry. Reviews in Mineralogy and Geochemistry. Mineralogical Society of America, Washington, DC, pp. 225–278.

Jacquet, S.H.M., Dehairs, F., Savoye, N., Obernosterer, I., Christaki, U., Monnin, C., Cardinal, D., 2008. Mesopelagic organic carbon remineralization in the Kerguelen Plateau region tracked by biogenic particulate Ba. Deep-Sea Research II, this issue [doi:10.1016/j.dsr2.2007.12.038].

Jeandel, C., Ruiz-Pino, D., Gjata, A., Poisson, A., Brunet, C., Charriaud, E., Dehairs, F., Delille, D., Fiala, M., Fravalo, C., Miquel, J.C., Park, Y.-H., Pondaven, P., Queguiner, B., Razouls, R., Shauer, B., Treguer, P., 1998. KERFIX, a time-series station in the Southern Ocean: a presentation. Journal of Marine Systems 17 (1–4), 555–570.

Jouandet, M.P., Blain, S., Metzl, N., Brunet, C., Trull, T.W., Obernosterer, I., 2008. A seasonnal carbon budget for a naturally iron-fertilized bloom over the Kerguelen Plateau in the Southern Ocean. Deep-Sea Research II, this issue [doi:10.1016/j.dsr2.2007.12.037].

Karsh, K.L., Trull, T.W., Lourey, M.J., Sigman, D.M., 2003. Relationship of nitrogen isotope fractionation to phytoplankton size and iron availability during the Southern Ocean Iron RElease Experiment (SOIREE). Limnology and Oceanography 48, 1058–1068.

Keller, K., Morel, F.M.M., 1999. A model of carbon isotopic fractionation and active carbon uptake in phytoplankton. Marine Ecology—Progress Series 182, 295–298.

King, P., Kennedy, H., Newton, P., Jickells, T., Brand, T., Calvert, S., Cauwet, G., Etcheber, H., Head, B., Khripounoff, A., Manighetti, B., Miquel, J.C., 1998. Analysis of total and organic carbon and total nitrogen in settling oceanic particles and marine sediment: an interlaboratory comparison. Marine Chemistry 60, 203–216.

Laws, E.A., Popp, B.N., Bidigare, R.R., Kennicutt, M.C., Macko, S.A., 1995. Dependence of phytoplankton carbon isotopic composition on growth rate and $[CO_2]_{aq}$: theoretical considerations and experimental results. Geochimica et Cosmochimica Acta 59 (6), 1131–1138.

Lefèvre, D., Guigue, C., Obernosterer, I., 2008. The metabolic balance at two contrasting sites in the Southern Ocean: The iron-fertilized Kerguelen area and HNLC waters. Deep-Sea Research II, this issue [doi:10.1016/j.dsr2.2007.12.006].

Lourey, M.J., Trull, T.W., 2001. Seasonal nutrient depletion and carbon export in the Subantarctic and Polar Frontal Zones of the Southern Ocean south of Australia. Journal of Geophysical Research 106 (C12), 31463–31488.

Lourey, M.J., Trull, T.W., Sigman, D.M., 2003. Sensitivity of the $\delta^{15}N$ of surface suspended and deep sinking particulate organic nitrogen to Southern Ocean seasonal nitrate depletion. Global Biogeochemical Cycles 17 (3), 1081.

Lourey, M.J., Trull, T.W., Tilbrook, B., 2004. Sensitivity of $\delta^{13}C$ of Southern Ocean suspended and sinking organic matter to temperature, nutrient utilisation and atmospheric CO_2. Deep-Sea Research I 51 (2), 281–305.

Lynch-Stieglitz, J., Stocker, T.F., Broecker, W.S., Fairbanks, R.G., 1995. The influence of air-sea exchange on the isotopic composition of oceanic carbon: observations and modeling. Global Biogeochemical Cycles 9 (4), 653–665.

Meredith, M.P., Heywood, K.J., Frew, R.D., Dennis, P.F., 1999. Formation and circulation of the water masses between the southern Indian Ocean and Antarctica: results from $\delta^{18}O$. Journal of Marine Research 57, 449–470.

Minagawa, M., Wada, E., 1984. Stepwise enrichment of ^{15}N along food chains: further evidence and the relation between $\delta^{15}N$ and animal age. Geochimica et Cosmochimica Acta 48, 1135–1140.

Mongin, M., Molina, E., Trull, T.W., 2008. Seasonality and scale of the Kerguelen plateau phytoplankton bloom: A remote sensing and modeling analysis of the influence of natural iron fertilization in the Southern Ocean. Deep-Sea Research II, this issue [doi:10.1016/j.dsr2.2007.12.039].

Mosseri, J., Quéguiner, B., Armand, L., Cornet-Barthaux, V., 2008. Impact of iron on silicon utilization by diatoms in the Southern Ocean: A case study of Si/N cycle decoupling in a naturally iron-enriched area. Deep-Sea Research II, this issue [doi:10.1016/j.dsr2.2007.12.003].

Needoba, J.A., Waser, N.A., Harrison, P.J., Calvert, S.E., 2003. Nitrogen isotopic fractionation in 12 species of marine phytoplankton during growth on nitrate. Marine Ecology Progress Series 255, 81–91.

Nodder, S.D., Charette, M.A., Waite, A.M., Trull, T.W., Boyd, P.W., Zeldis, J., Buesseler, K.O., 2001. Particle transformations and export flux during an *in situ* iron-stimulated bloom in the Southern Ocean. Geophysical Research Letters 28 (12), 2409–2412.

O'Leary, T., Trull, T.W., Griffiths, F.B., Tilbrook, B., Revill, A.T., 2001. Euphotic zone variations in bulk and compound-specific δ13C of suspended organic matter in the subantarctic ocean, south of Australia. Journal of Geophysical Research 106 (C12), 31669–31689.

Obernosterer, I., Christaki, U., Lefèvre, D., Catala, P., Van Wambeke, F., Le Baron, P., 2008. Rapid bacterial mineralization of organic carbon produced during a phytoplankton bloom induced by natural iron fertilization in the Southern Ocean. Deep-Sea Research II, this issue [doi:10.1016/j.dsr2.2007.12.005].

Olson, R.J., 1981. Differential photoinhibition of marine nitrifying bacteria: a possible mechanism for the formation of the primary nitrite maximum. Journal of Marine Research 39, 227–238.

Park, Y.-H., Fuda, J.-L., Durand, I., Naveira Garabato, A.C., 2008a. Internal tides and vertical mixing over the Kerguelen Plateau. Deep-Sea Research II, this issue [doi:10.1016/j.dsr2.2007.12.027].

Park, Y.-H., Roquet, F., Durand, I., Fuda, J.-L., 2008b. Large scale circulation over and around the Northern Kerguelen Plateau. Deep-Sea Research II, this issue [doi:10.1016/j.dsr2.2007.12.030].

Peeken, I., Hoffmann, L.J., Assmy, P., Bathmann, U., Croot, P.L., Harbou, L., Henjes, J., Jansen, S., Kraegefsky, S., Lochte, K., Sachs, O., Sauter, E., 2006. Effect of in situ Iron Fertilisation During Contrasting Seasons—Comparison Between EisenEx and EIFEX. ASLO-TOS-AGU Ocean Sciences Meeting Abstract, OS32A-06.

Popp, B.N., Laws, E.A., Bidigare, R.R., Dore, J.E., Hanson, K.L., Wakeham, S.G., 1998. Effect of phytoplankton cell geometry on carbon isotopic fractionation. Geochimica et Cosmochimica Acta 62 (1), 69–77.

Popp, B.N., Trull, T., Kenig, F., Wakeham, S.G., Rust, T.M., Tilbrook, B., Griffiths, F.B., Wright, S.W., Marchant, H.J., Bidigare, R.R., Laws, E.A., 1999. Controls on the carbon isotopic composition of Southern Ocean phytoplankton. Global Biogeochemical Cycles 13 (4), 827–843.

Rau, G.H., Teyssie, J.-L., Rassoulzadegan, F., Fowler, S.W., 1990. $^{13}C/^{12}C$ and $^{15}N/^{14}N$ variations among size fractionated marine particles: implications for their origin and trophic relationships. Marine Ecology Progress Series 59, 33–38.

Rau, G.H., Riebesell, U., Wolf-Gladrow, D., 1997. CO_{2aq}-dependent photosynthetic ^{13}C fractionation in the ocean: a model versus measurements. Global Biogeochemical Cycles 11 (2), 267–278.

Rutgers van der Loeff, M., Vöge, I., 2001. Does Fe fertilisation enhance the export production as measured through the $^{234}Th/^{238}U$ disequilibrium in surface water? In: Smetacek, V., Bathmann, U., El Naggar, S. (Eds.), The expeditions ANTARKTIS XVIII/1-2 of the Research Vessel Polarstern in 2000. Berichte zur Polar- und Meeresforschnung 400. Alfred-Wegener Institute, Bremerhaven, Germany, pp. 222–225.

Savoye, N., Trull, T.W., Jacquet, S.H.M., Navez, J., Dehairs, F., 2008. ^{234}Th-based export fluxes during a natural iron fertilisation experiment in the Southern Ocean (KEOPS). Deep-Sea Research II, this issue [doi:10.1016/j.dsr2.2007.12.036].

Sedwick, P.N., DiTullio, G.R., 1997. Regulation of algal blooms in Antarctic Shelf waters by the release of iron from melting sea ice. Geophysical Research Letters 24, 2515–2518.

Sedwick, P.N., DiTullio, G.R., Hutchins, D.A., Boyd, P.W., Griffiths, F.B., Crossley, A.C., Trull, T.W., Queguiner, B., 1999. Limitation of algal growth by iron deficiency in the Australian Subantarctic region. Geophysical Research Letters 26 (18), 2865–2868.

Sedwick, P.N., Blain, S., Queguiner, B., Griffiths, F.B., Fiala, M., Bucciarelli, E., Denis, M., 2002. Resource limitation of phytoplankton growth in the Crozet Basin, Subantarctic Southern Ocean. Deep-Sea Research II 49, 3327–3349.

Sigman, D.M., Boyle, E.A., 2000. Glacial/interglacial variations in atmospheric carbon dioxide. Nature 407, 859–869.

Sigman, D.M., Altabet, M.A., Francois, R., McCorkle, D.C., Gaillard, J.-F., 1999a. The isotopic composition of diatom-bound nitrogen in Southern Ocean sediments. Paleoceanography 14, 118–134.

Sigman, D.M., Altabet, M.A., McCorkle, D.C., Francois, R., Fischer, G., 1999b. The $\delta^{15}N$ of nitrate in the Southern Ocean: consumption of nitrate in surface waters. Global Biogeochemical Cycles 13 (4), 1149–1166.

Sigman, D.M., Altabet, M.A., McCorkle, D.C., Francois, R., Fischer, G., 2000. The $\delta^{15}N$ of nitrate in the Southern Ocean: nitrogen cycling and circulation in the ocean interior. Journal of Geophysical Research 105 (C8), 19599–19614.

Sigman, D.M., Casciotti, K.L., Andreani, M., Barford, C., Galanter, M., Bohlke, J.K., 2001. A bacterial method for the nitrogen isotopic analysis of nitrate in seawater and freshwater. Analytical Chemistry 73, 4145–4153.

Sigman, D.M., Granger, J., DiFiore, P.J., Lehmann, M.M., Ho, R., Cane, G., van Geen, A., 2005. Coupled nitrogen and oxygen isotope measurements of nitrate along the eastern North Pacific margin. Global Biogeochemical Cycles 19, GB4022.

Timmermans, K.R., Stolte, W., de Baar, H.J.W., 2004. Iron-mediated effects on nitrate reductase in marine phytoplankton. Marine Biology 121 (2), 389–396.

Tortell, P.D., Rau, G.H., Morel, F.M.M., 2000. Inorganic carbon acquisition in coastal Pacific phytoplankton communities. Limnology and Oceanography 45 (7), 1485–1500.

Tréguer, P., LeCorre, P., 1975. Manuel d'analyse des sels nutritifs dans l'eau de mer. Utilisation de l'AutoAnalyser II Technicon, second ed. Univ. Bretagne Occidentale, Laboratoire de Chimie marine, Brest, France.

Trull, T.W., Armand, L., 2001. Insights into Southern Ocean carbon export from the $\delta^{13}C$ of particles and dissolved inorganic carbon during the SOIREE iron fertilisation experiment. Deep-Sea Research II 48 (11/12), 2655–2680.

Trull, T.W., Bray, S.G., Manganini, S.J., Honjo, S., François, R., 2001a. Moored sediment trap measurements of carbon export in the Subantarctic and Polar Frontal Zones of the Southern Ocean, south of Australia. Journal of Geophysical Research 106 (C12), 31489–31510.

Trull, T.W., Rintoul, S.R., Hadfield, M., Abraham, E.R., 2001b. Circulation and seasonal evolution of Polar waters south of Australia: implications for iron fertilisation of the Southern Ocean. Deep-Sea Research II 48 (11/12), 2439–2466.

Waite, A.M., Safi, K.A., Hall, J.A., Nodder, S.D., 2000. Mass sedimentation of picoplankton embedded in organic aggregates. Limnology and Oceanography 45 (1), 87–97.

Waser, N.A., Yu, Z., Yin, K., Nielsen, B., Harrison, P.J., Turpin, D.H., Calvert, S.E., 1999. Nitrogen isotopic fractionation during a simulated diatom spring bloom: importance of N-starvation in controlling fractionation. Marine Ecology Progress Series 179, 291–296.